INVESTIGATING FEEDBACK AND RELAXATION IN CLUSTERS OF
GALAXIES WITH THE CHANDRA X-RAY OBSERVATORY

By

Kenneth W. Cavagnolo

AN ABSTRACT OF A DISSERTATION

Submitted to
Michigan State University
in partial fulfillment of the requirements
for the degree of

DOCTOR OF PHILOSOPHY

Department of Physics and Astronomy

2008

Dr. Megan Donahue

ABSTRACT

INVESTIGATING FEEDBACK AND RELAXATION IN CLUSTERS OF
GALAXIES WITH THE CHANDRA X-RAY OBSERVATORY

By

Kenneth W. Cavagnolo

This is where the abstract will go. But for now, let's... DANCE DANCE DANCE!

INVESTIGATING FEEDBACK AND RELAXATION IN CLUSTERS OF
GALAXIES WITH THE CHANDRA X-RAY OBSERVATORY

By

Kenneth W. Cavagnolo

A DISSERTATION

Submitted to
Michigan State University
in partial fulfillment of the requirements
for the degree of

DOCTOR OF PHILOSOPHY

Department of Physics and Astronomy

2008

ABSTRACT

INVESTIGATING FEEDBACK AND RELAXATION IN CLUSTERS OF
GALAXIES WITH THE CHANDRA X-RAY OBSERVATORY

By

Kenneth W. Cavagnolo

This is where the abstract will go. But for now, let's... DANCE DANCE DANCE!

Dedicated to my mother: Miss Lorna Lorraine Cox.

ACKNOWLEDGMENTS

Thanks to Christopher Waters for the LaTeX class used to format this thesis.

My deepest thanks to Megan Donahue and Mark Voit for their guidance, wisdom, patience, and without whom I would be in quantum computing. I can only say, "Thank you, Megan" for giving me the time and space to find my bearings after my mother's passing, words are insufficient to express my gratitude. Ming Sun always listened, always had time for a question, and was never wrong. Jack Baldwin nutured my painfully slow development as a research assistant, a more calming voice there has never been. On behalf of everyone that has never said so, "We love you, Shawna Prater. MSU Astronomy and Astrophysics cannot do business without you." And of course, Debbie Simmons, without whom I would have been dropped from all courses and locked out of the building.

Many dissertations across many disciplines acknowledge many religious figures and a multitude of gods; but what about the Sun? Every time I feel the startling warmth of the Sun on my skin, it is an invigorating experience. To be bathed in photons millions of years old from an inconceivably large nuclear power plant over a hundred million kilometers away makes me feel connected to the Universe in a way that is surreal. To feel purposely cared for by an absentee whom's existance and operation are fundamentally devoid of purpose is quite profound. Unknowingly, the Sun gave rise to a species of sentient dissadents. For that I say, "Thank you, Sun!"

To my wife: Our vows were fortelling, I will indeed require the course of an entire life to express my appreciation for the tenderness, care, love, and humor you gave during completion of this dissertation. You are, and always will be, my beloved.

PREFACE

Our Universe is predominantly an untold story. Within a larger, nested framework of complex mechanisms, humans evolved with minimal impact on the systems which support and nurture our existance. Yet, during the short era of global industrialization, we have compromised the effectiveness and function of the systems which formed the biodiversity which makes our planet such a wonderful place. As an acknowledgement of the appreciation our species has for the Earth, and as a show of our understanding for humanity's fleeting presence in the Earth's lifecycle, let us strive to utilize the pursuit of knowledge, through application of reason and logic, so that our actions benefit "all the children, of all species, for all of time" (McDonough & Braungart, 2002). Let us all exert effort such that the Earth and the Universe will be enriched by humanity, and that our actions – local, global, and possibly interplanetary – will leave the places we inhabit and visit nourished from our presence.

TABLE OF CONTENTS

LIST OF TABLES

LIST OF FIGURES

Chapter 1:
Introduction

1.1 Clusters of Galaxies

Of the luminous matter in the Universe, stars and galaxies are often the most familiar to a sky gazer. Aside from the Moon and the occasional bright planet, stars are the most abundantly obvious patrons of the night sky. Viewed from a sufficiently dark location, the stars form a band of light interspersed with dust and gaseous clouds which define the Milky Way, our home galaxy. The Milky Way is only one of more than 30 galaxies in a gravitationally bound group of galaxies, named the Local Group, which includes the well-known, nearby galaxy Andromeda. But in cosmological terms, the Local Group is very small in comparison to immense structures containing thousands of galaxies. In a turn of wit, these structures are appropriately named clusters of galaxies, and are the focus of this dissertation.

Galaxy clusters are the most massive gravitationally bound structures to have yet formed in the Universe. As where galaxy groups have roughly 10-50 galaxies, galaxy clusters have hundreds to thousands of galaxies. When viewed with a telescope, a galaxy cluster appears as a tight distribution of mostly elliptical and S0 spiral galaxies within a radius of $\sim 1 - 5$ Mpc[1] of each other. Rich galaxy cluster are truly spectacular objects, as can be seen in Figure 1.1 which shows the *Hubble* Space Telescope's close-up of the strong lensing cluster Abell 1689.

---

[1]Throughout this dissertation, a flat ΛCDM cosmogony of $H_0 = 70$ km s^{-1} Mpc^{-1} (h_{70}=1), $\Omega_\Lambda = 0.7$, and $\Omega_M = 0.3$ is assumed
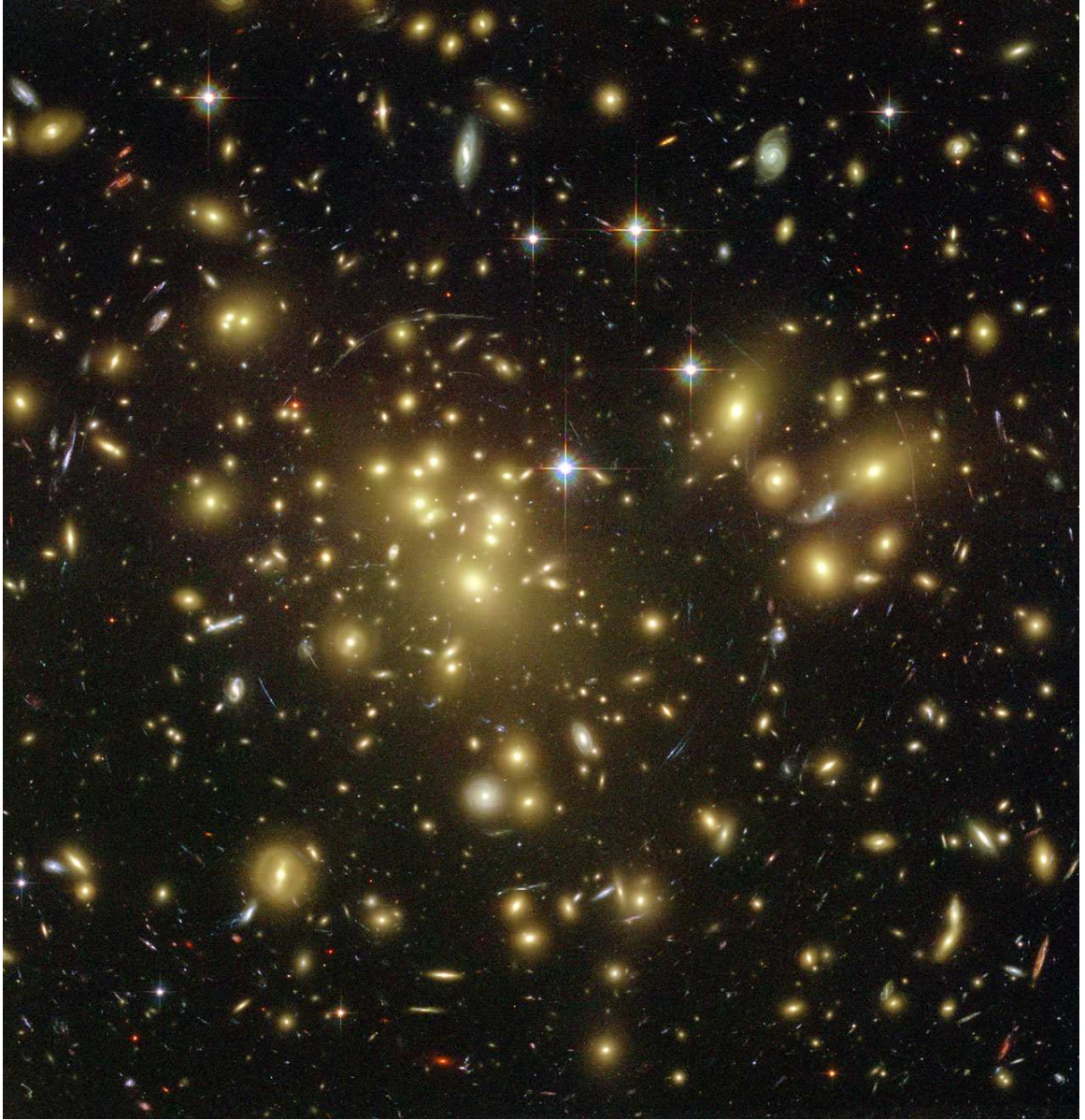
Figure 1.1 Shown here is an optical image of the galaxy cluster Abell 1689 as observed with the ACS instrument onboard the *Hubble* Space Telescope. The fuzzy yellowish spheres are giant elliptical (gE) galaxies in the cluster, with the gE nearest the center of the image being the brightest cluster galaxy – ostensibly, the cluster "center". Image taken from NASA's Hubblesite.org. Per NASA copyright policy: "NASA material is not protected by copyright unless noted". Image Credits: NASA, N. Benitez (JHU), T. Broadhurst (The Hebrew University), H. Ford (JHU), M. Clampin(STScI), G. Hartig (STScI), G. Illingworth (UCO/Lick Observatory), the ACS Science Team and ESA.

Galaxy clusters are deceptively named. As with most objects in the Universe, one of the most revealing characteristics of an object is its mass, and the mass of clusters of galaxies are not dominated by galaxies. With the proper vision, an observer would find clusters are dominated ($\gtrsim 70\%$) by dark matter with most ($\gtrsim 80\%$) of the baryonic mass[2] in the form of a hot ($kT \approx 2 - 15$ keV; 10-100 million degrees), luminous (10^{43-46} ergs s^{-1}), diffuse ($10^{-1} - 10^{-4} cm^{-3}$) intracluster medium (ICM) which is cospatial with the galaxies but dwarfs them in mass. For comparison, the ICM, on average, is 10^{20} times less dense than typical Earth air, 10^5 times denser than the mean cosmic density, more than 2000 times hotter than the surface of the Sun, and shines as bright as 10^{35} 100 watt lightbulbs.

Because of the ICM's extreme temperature, the gas is mostly ionized, making it a plasma. For the temperature range of clusters, the ICM is most luminous at X-ray wavelengths of the electromagnetic spectrum. This makes observing galaxy clusters with X-ray telescopes, like NASA's *Chandra* X-ray Observatory, a natural choice. Clusters have masses ranging over 10^{14-15} M$_\odot$ with velocity dispersions of 500-1500 km/s [ref]. The ICM has also been enriched with metals (meaning any element with a $Z > 2$) to an average value of ~ 0.3 Solar abundance. Shown in Figure 1.2 is an optical, X-ray, and gravitational lensing composite image of the galaxy cluster 1E0657-56. This cluster is undergoing an especially spectacular and rare merger which allows for the separate dominant components of a cluster – dark matter, the ICM, and galaxies – to be "seen" distinctly.

Knowing the characteristics of galaxy clusters is a small part of the discovery process, we must also wonder, why study clusters of galaxies? Galaxy clusters have two very important roles in the current research paradigm:

1) The cluster gravitational potential well is deep enough to retain all the matter which has fallen in over the age of the Universe. This slowly evolving 'sealed box'

---

[2]Baryonic matter is a handy term for ordinary matter like an kind of atom, while non-baryonic matter is more exotic like free electrons or dark matter particles.
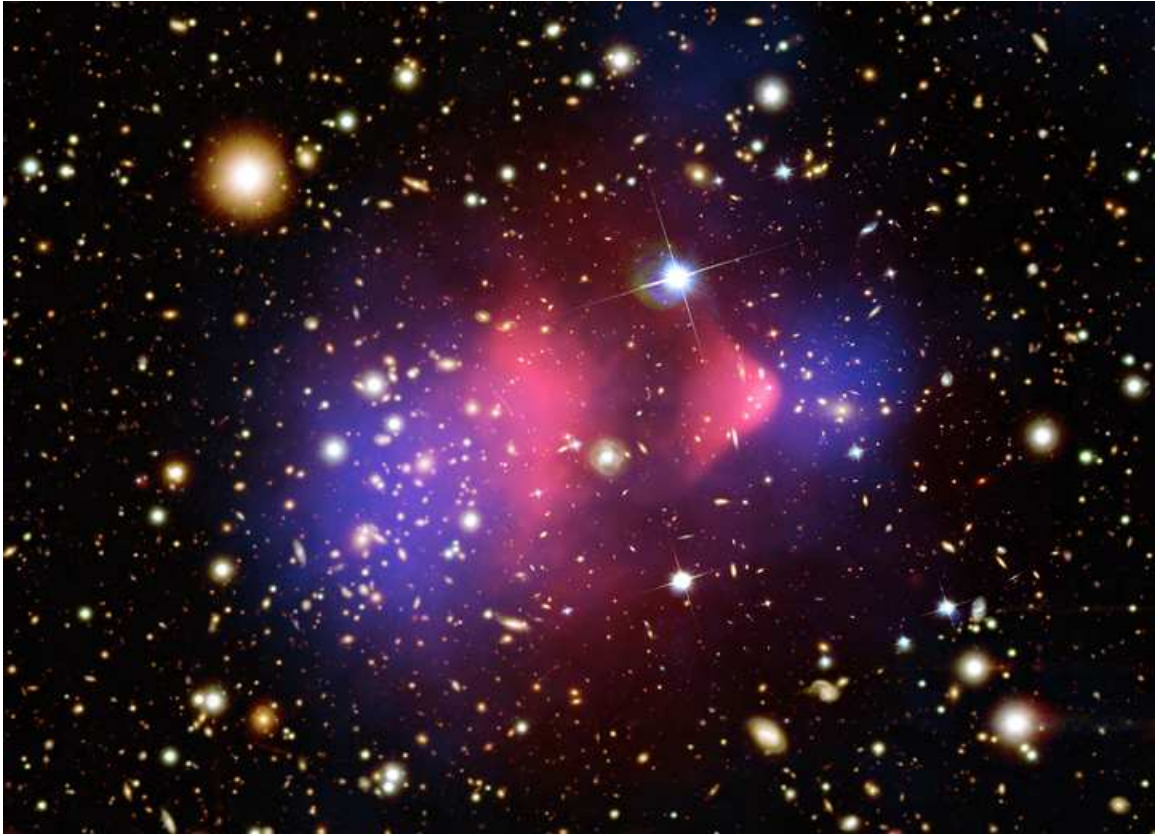
Figure 1.2 This image shows the galaxy cluster 1E0657-56, aka the Bullet Cluster. All of the primary components of a galaxy cluster can be seen in this image: the X-ray ICM (pink), dark matter (blue), and galaxies. The brillant white object with diffraction spikes is a star. This cluster has become very famous because it is direct evidence for the existance of dark matter (Clowe et al., 2006). Image taken from NASA Press Release 06-297. Per NASA copyright policy: "NASA material is not protected by copyright unless noted". Image credits: NASA/CXC/CfA/Markevitch et al. (2002) (X-ray); NASA/STScI/Magellan/U.Arizona/Clowe et al. (2006) (Optical); NASA/STScI/ESO WFI/Magellan/U.Arizona/Clowe et al. (2006) (Lensing).

therefore contains a comprehensive history of all the physical processes involved in galaxy formation and evolution, such as stellar evolution, supernovae feedback, black hole activity in the form of active galactic nuclei, galaxy mergers, ram pressure stripping of infalling galaxies and groups, and so on. The ICM acts as a record-keeper of all this activity, and by studying the ICM's physical properties, the thermal history of the cluster can be partially recovered. This in turn, hopefully, can aide in forming a better understanding of hierarchical structure formation. More specifically, clusters are a means to exploring the processes which have given rise to the variety of galaxies found in the Universe (condensed into the morphological classifications of the Hubble Sequence shown in Figure 1.3) and possibly understanding how galaxies evolve.

2) Galaxy clusters represent a unique tracer of the Universe's underlying cosmological parameters, including the nature of dark matter and the dark energy equation of state. Large-scale structure growth is exponentially sensitive to some of these parameters, and by counting the number of clusters found in a comoving volume of space, specifically above a given mass threshold, clusters may be very useful in cosmological studies (**?**). In this dissertation I circuitously address both of the points.

While clusters have their specific uses in particular areas of astrophysics research, they also are inherently interesting objects. Very few areas of physics are unused when studying galaxy clusters. A full-blown, theoretical construction of a galaxy cluster requires, to name just a few: gravitation, fluid mechanics, thermodynamics, hydrodynamics, magnetohydrodynamics, and high-energy/particle/nuclear physics. Multiwavelength observations of galaxy clusters provide excellent datasets for testing the theoretical predictions from other areas of physics, and clusters are also a unique laboratory for empirically establishing how different areas of physics interconnect. Just this aspect of clusters puts them in a special place among the objects in our Universe worth intense, time-consuming, (and sometimes expensive) scrutiny. At a minimum, galaxy clusters are most definitely worthy of being the focus of a humble
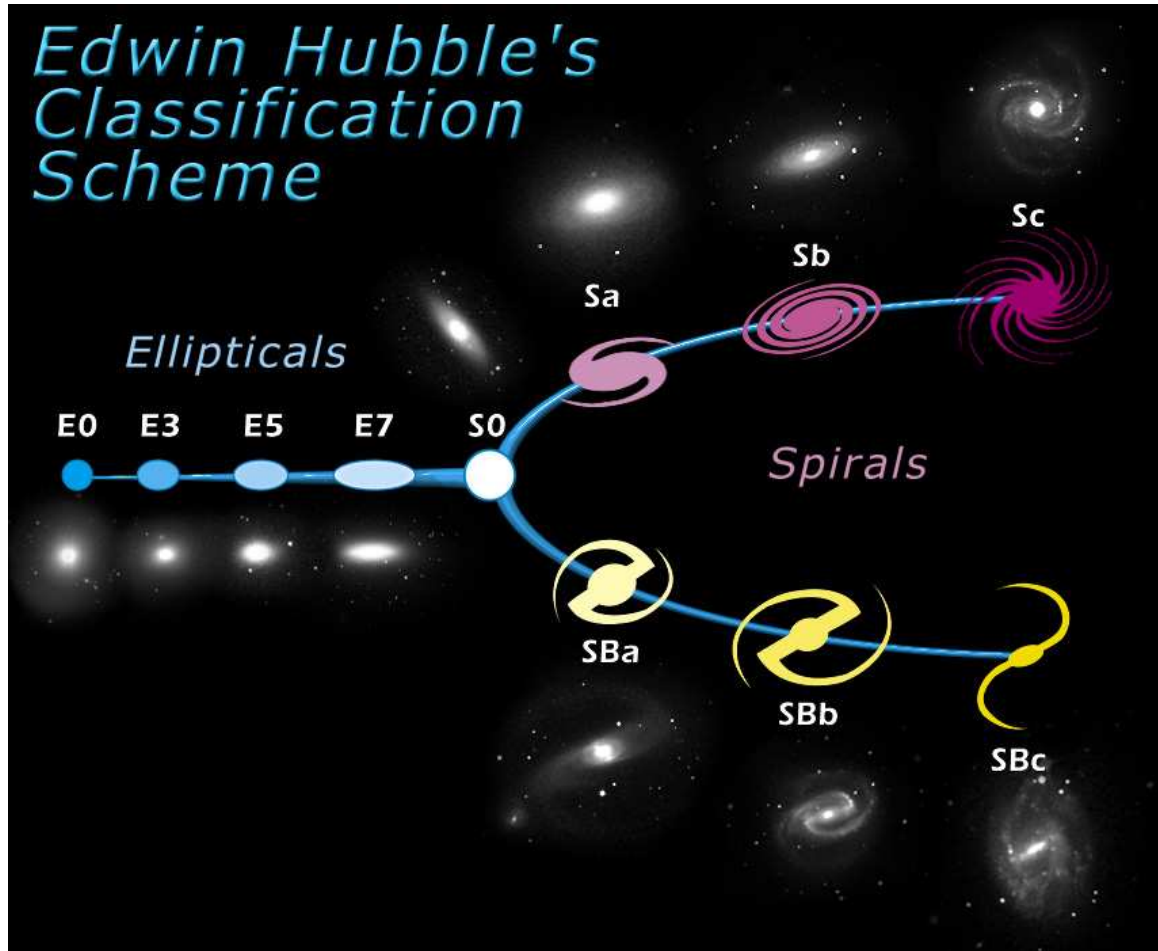
Figure 1.3 Shown here is the Hubble Sequence which conveys the basic (albeit over-simplified) concept that galaxy morphologies are related in some way. While a by-eye assesment is how these galaxies where placed in this order, fundamentally understanding the physical machinery which explains this diagram is still a work in progress. A portion of this dissertation focuses on the process of massive galaxy formation, and in a way is aimed at developing a better understanding of how, for example, an E0 is related to an E7. Image taken from NASA Press Release STScI-1999-34. Per NASA copyright policy: "NASA material is not protected by copyright unless noted".

dissertation from an fledgling astrophysicist.

In the following sections of this chapter I more thoroughly discuss specific reasons for studying clusters of galaxies which gave root to this dissertation: the unresolved issues of the "cooling flow problem" and why clusters of different masses are not simply scaled versions of one another. As this is a dissertation focused around observational work, I also provide a brief primer on the X-ray observable properties of clusters which are important to understanding this dissertation. This is followed by a discussion of gas entropy, a physical property of the ICM which may be unfamiliar to many readers and is utilized heavily in Chapters 3 and 4. The chapter concludes with a very cursory description of the *Chandra* X-ray Observatory (CXO), the space-based telescope with which all of the data presented in this dissertation was collected.

1.2 The Incomplete Picture of Clusters

The literature on galaxy clusters is extensive. There has been a great deal already written about clusters (with much more eloquence), and I strongly suggest reading Mushotzky (1984); Kaiser (1986, 1991); Sarazin (1986); Fabian (1994); Voit (2005); Peterson & Fabian (2006); Markevitch & Vikhlinin (2007); McNamara & Nulsen (2007) (and references therein) for a comprehensive review of the concepts and topics to be covered in this dissertation. But history aside, what is already known about clusters is not that interesting a research topic. This section focuses on a few unresolved mysteries involving galaxy clusters: the cooling flow problem as it relates to galaxy formation and the breaking of self-similarity in relation to using clusters in cosmological studies.

1.2.1 The Cooling Flow Problem

In many galaxy clusters densest and coolest ICM gas is found at the very bottom of the cluster graviational potential well. In these same clusters the bottom of the

7

cluster potential is not surprisingly the location of the largest and most massive galaxy in the cluster, the brightest cluster galaxy (BCG). The radiative cooling time of the ICM in the dense, cool core region is much shorter than the age of the Universe, *e.g.* $t_{\rm cool} \ll H_0^{-1}$, and shorter than the age of the cluster. However, $t_{\rm cool}$ is longer than the gravitational free-fall time (Peterson & Fabian, 2006). Thus, it follows that the ICM in the cluster core has undergone extended periods of cooling during the cluster lifetime. Since the ICM radiates away copious amounts of thermal energy in the form of X-ray emission, the temperature of radiating gas subsequently decreases. But, the internal pressure of a cooling ideal gas (an appropriate approximation for the ICM) must also decrease. Hence, the ICM which is cooling fastest (the gas in the core) does not provide sufficient pressure support of overlying gas layers which are cooling more slowly and the resulting pressure imbalance should result in a subsonic flow of cool gas into the cluster core. This is the most simplistic model of a cluster "cooling flow" (see Fabian 1994 and Peterson & Fabian 2006 for reviews).

The main cooling mechanism in the cooling flow, X-ray emission, proceeds at a rate proportional to the square of the gas density, $\epsilon \propto \rho^2$, where ϵ is emissivity and ρ is gas density. In addition, the cooling flow mass deposition rate is $\dot{M} \propto L_{bol} T^{-1}$ where L_{bol} is bolometric luminosity[3] and T is gas temperature. Taking these two relations together, it is obvious that as the density of the cooling region increases so to does the mass deposition rate, *e.g.* the cooling flow process acts within a positive feedback cycle.

As the cooling flow region grows in size it eventually encompasses the BCG. But the infalling gas of the cooling flow is not expected to be laminar, continuous, or in thermodynamic equilibrium with the ambient medium. Under these conditions thermal instabilities are expected to rapidly form and in some circumstances collapse to form by-products such as gaseous molecular clouds and stars. Since the BCG is

---

[3]Bolometric luminosity in this context means the integrated luminosity over all wavelengths, for example $E = 0.001 - 100.0$ keV

cospatial with the cooling flow and its by-products, one predicted consequence for the evolution of BCGs is that, irrespective of cosmic time, BCGs should be continually replenished with young, blue stellar populations and supremely massive. One should then expect the cores of clusters suspected of hosting a cooling flow to have gigantic, blue BCGs bathed in clouds of emission line nebulae. However, observations of cooling flow clusters reveal the true nature of the core to be quite to the contrary.

The optical properties of BCGs have been known for quite a long time [ref] and these massive galaxies are neither as blue, bright, or massive as would be expected from the extended periods of growth from continual mass accretion via cooling flows. While attempts were made in the past to selectively channel the unobserved cool gas into optically dark objects, such as in low-mass, distributed star formation, methodical searches in the optical [ref], infrared [ref], UV [ref], radio [ref], and soft X-ray [ref] wavelengths have revealed that the total mass of gas associated with cooling flows is much less than expected [ref]. Furthering the case that cooling flows are not as advertised, *XMM-Newton* RGS X-ray spectroscopy of clusters expected to host very massive cooling flows definitively proved that the ICM was not cooling to temperatures less than 1/3 of the cluster virial temperature (Peterson et al., 2001; Tamura et al., 2001). A discontinuous cooling X-ray medium does not occur in simple single-phase cooling flow models without a troubling amount of fine-tuning, for example by adding turbulent mixing to the multi-phase cooling flow model (Thomas et al., 1987).

All of the observational evidence has resulted in a two-component "cooling flow problem": 1) spectroscopy of soft X-ray emission from cooling flow clusters is inconsistent with theoretical predictions, and 2) multiwavelength observations reveal a lack of mass-sinks at the tail-end of the enormous theoretical mass deposition rates of cooling flows. This begs the simple question: where has all the cool gas gone? As is the case with most questions, the best answer thus far was simple: the ICM has been heated, reducing cooling flow rates. But what feedback mechanisms are responsible

for ~~retarding~~ cooling in cluster cores? How do these mechanisms operate? What observational constraints can we find to determine which combination of feedback mechanism hypotheses are correct?

The cores of clusters are active places, so finding heating mechanisms is not too difficult. However, there is an impendance mismatch in heating and cooling processes which limits the list of sources capable of supplying sufficient heat to the ICM. Radiative cooling proceeds as the square of gas density, whereas heating is proportional to volume. This makes compensating for radiative cooling losses over an $\approx 10^6$ kpc^3 volume, where the radial density can change by four orders of magnitude, quite difficult. The best proposed solution to the cooling flow problem thus far invokes outbursts from the active galactic nucleus (AGN) in the BCG (Churazov et al., 2002; Brüggen & Kaiser, 2002; Brüggen et al., 2002; Ruszkowski & Begelman, 2002; Alexander, 2002; Omma et al., 2004; McCarthy et al., 2004; Roychowdhury et al., 2004; Hoeft & Brüggen, 2004; Dalla Vecchia et al., 2004; Soker & Pizzolato, 2005; Pizzolato & Soker, 2005; Voit & Donahue, 2005).

The basic model of how AGN feedback works is that first gas accretes onto a supermassive black hole at the center of the BCG, resulting in the acceleration and ejection of very high energy particles back into the cluster environment. The energy released in an AGN outburst is of order 10^{58-61} ergs. Under the right conditions, and via ~~a~~ poorly understood mechanism, the ~~feedback~~ energy is transferred to the ICM and thermalized thereby heating the gas. The details of how this process operates is beyond the scope of this dissertation (see McNamara & Nulsen 2007 for a ~~nice~~ review). As noted, AGN outburst energy does not magically heat the ICM, the heat must be transferred to the ICM and then azimuthally distributed.

~~In Chapter 3 results are presented which show that ICM entropy has been altered in ways which are consistent with AGN feedback models. Entropy and its connection to AGN feedback is discussed in Subsection 1.3.2 of this Introduction. In Chapter~~

4 I also present results which suggest that electron thermal conduction may be an important mechanism in distributing AGN feedback energy. Hence, this dissertation, in small part, seeks to add to the understanding of how feedback functions in clusters, and thus how to resolve the cooling flow problem. The resolution of which will lead to better models of galaxy formation and evolution.

1.2.2 BREAKING OF SELF-SIMILARITY

We now know the evolution of, and structure within, the Universe are a direct result of the influence from dark energy and dark matter. ~~Even though it is not understood,~~ an all pervading repulsive dark energy ~~is~~ responsible for the accelerating expansion of the Universe (Riess et al., 1998, 2007) ~~and ultimately controls the fate of the Universe (see Krauss & Scherrer 2007 for some interesting speculations).~~ Dark matter is an unknown form of matter which interacts with itself and ordinary matter (both baryonic and non-baryonic) ~~predominantly~~ through gravitation. Until ~~recently,~~ the influence of dark matter on the Universe has been greater than that of dark energy, this is evident from the existance of large-scale structure like galaxy clusters

An end result of the gravitational attraction between large amalgamations of dark matter particles, called dark matter halos, is the merger of small halos into ever larger halos. Since dark matter far outweighs baryonic matter in the Universe, the baryons are coupled to the dark matter halos via gravity, and hence are dragged along during the halo merger process. Like raindrops falling in a pond that drains into a river which flows into the ocean, the process of smaller units merging to create larger units is found *ad infinitum* in the Universe and is given the name hierarchical structure formation. A useful visualization of the hierarchical structure formation process is shown in Fig. 1.4. Hierarchical formation begins with small objects like the first stars, continues on to galaxies, and culminates in the largest present objects, clusters of galaxies.

In a very simplistic redux, dark energy is attempting to push space apart while dark matter is attempting to pull matter together within that space. Were the balance and evolution of dark energy and dark matter weighted heavily toward one or the other it becomes clear that the amount of structure and its distribution will be different. Thus, the nature of dark matter and dark energy ultimately influence the number of clusters found at any given redshift (*e.g.* White et al. 1993) and hence cluster number counts are immensely powerful in determining cosmological parameters (*e.g.* Borgani et al. 2001).

Individual clusters do not yield the information necessary to study the underlying cosmogony. However, the number density of clusters above a given mass threshold within a given redshift range (the so-called cluster mass function) is a useful quantity Voit (2005). But the cluster mass function is a powerful cosmological tool only if cluster masses can be accurately measured. With no direct method of measuring cluster mass, easily observable properties of clusters must be used as proxies to infer mass. Reliable mass proxies such as cluster temperature and luminosity arise naturally from the theory that clusters are scaled versions of each other, yielding low-scatter scaling relations (Kaiser, 1986, 1991; Evrard & Henry, 1991). Mass-observable relations, such as mass-temperature and mass-luminosity, derive from the fact that most clusters are virialized, meaning the cluster's energy is shared such that the virial theorem, $-2\langle T \rangle = \langle V \rangle$, is a valid approximation. Both theoretical (Evrard et al., 1996; Bryan & Norman, 1998; Mohr et al., 1999; Bialek et al., 2001; Borgani et al., 2002) and observational (Mushotzky, 1984; Edge & Stewart, 1991; Allen & Fabian, 1998a; Arnaud & Evrard, 1999; Finoguenov et al., 2001) studies have shown cluster mass correlates well with X-ray temperature and luminosity, but that there is much larger ($\approx 20 - 30\%$) scatter in these relations than predicted. The breaking of self-similarity is attributed to non-gravitational processes such as ongoing mergers, heating via feedback, or radiative cooling in the cluster core (Cavaliere et al., 1999;
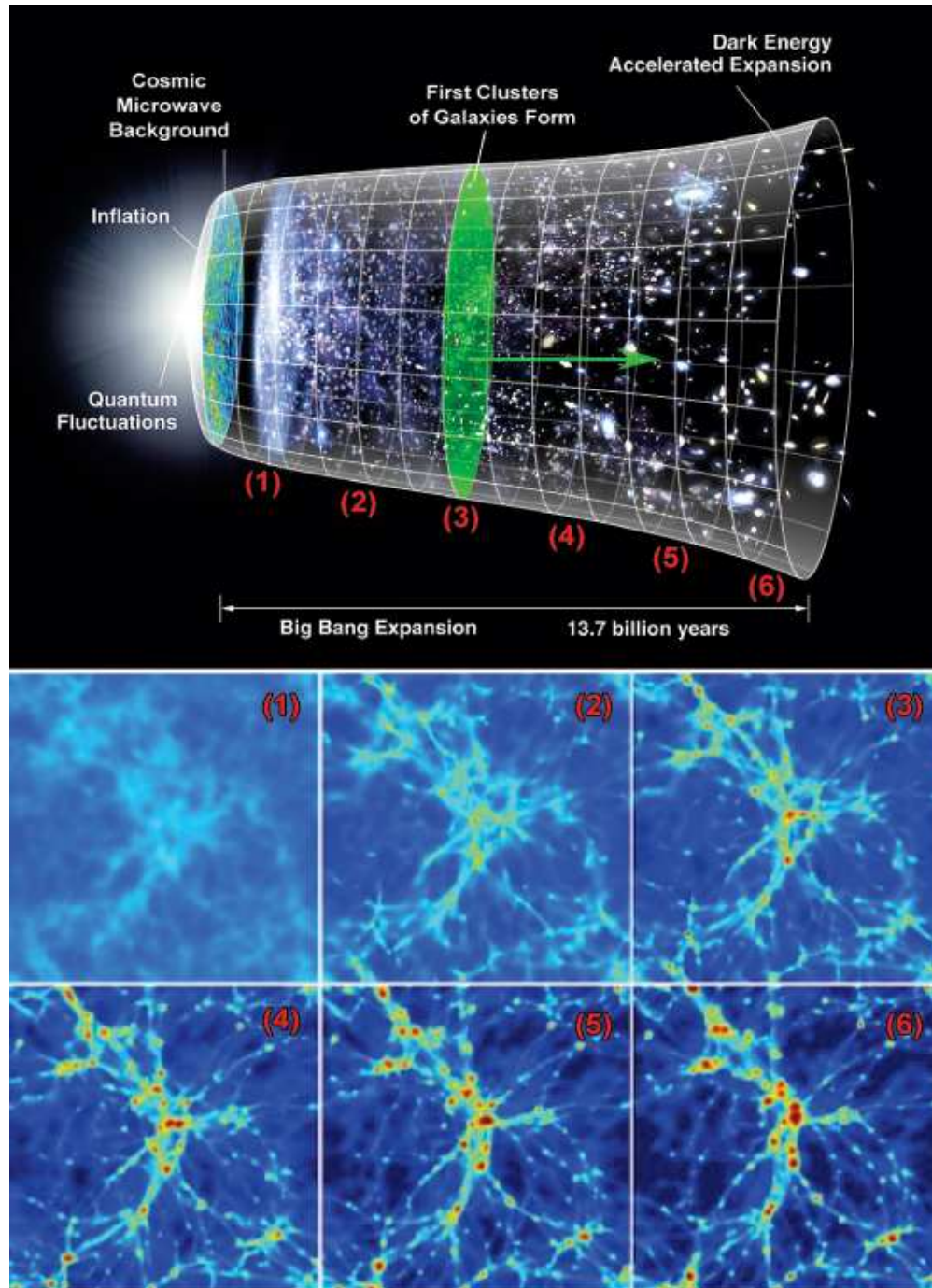
Figure 1.4 Shown here are an illustration of hierarchical structure formation and snapshots from the simualtion a galaxy cluster forming. The cluster snapshots are numbered on the illustration at the approximate time each stage of cluster collapse occurs. Notice that, at first, very small objects collapse and then these smaller objects slowly merge into much larger halos. Illustration taken from NASA/WMAP Science Team and modified by author. Simulation snapshots taken from images distributed to the public by the Virgo Consortium: http://www.virgo.dur.ac.uk

Bower et al., 2001; Voit & Bryan, 2001; Voit et al., 2002).

To reduce the scatter in scaling-relations and increase their utility for weighing clusters, how secondary processes alter temperature and luminosity must be quantified and then accounted for. It was predicted that clusters with a high-degree of spatial uniformity and symmetry (*e.g.* clusters with the least substructure in their dark matter and gas distributions) would be the most relaxed and have the smallest deviations from mean mass-observable relations. This is concept quite prevalent in many natural systems, such as a placid lake or spherical gas cloud of uniform density and temperature. Structural analysis of cluster simulations, for example the recent work of Jeltema et al. (2007) or Ventimiglia et al. (2008), have shown measures of substructure correlate well with cluster dynamical state. But spatial analysis is at the mercy of perspective. If equally robust aspect-independent measures of dynamical state could be found, then quantifying deviation from mean mass-scaling relations would be improved and the uncertainty of inferred cluster masses could be further reduced. This ultimately would lead to a more accurate cluster mass function and by extension the constraints on theories explaining dark matter and dark energy could grow tighter.

In Chapter 2 I present work investigating ICM temperature inhomogeneity, which has been proposed as a method for better understanding the dynamical state of a cluster (**?**). Temperature inhomogeneity has the advantage of being a spectroscopic quantity and therefore falls into the class of aspect-independent metrics which may be useful for reducing scatter in mass-observable relations. ~~So in a very circuitous manner, this dissertation might contribute to the development of a very modest improvement to our understanding of the Universe's make-up and evolution. Sometimes even the seeming obscure advancement of knowledge in one area is important.~~

1.3 THE INTRACLUSTER MEDIUM

In the Introduction, the ICM was presented as a mostly ionized, hot, diffuse plasma which dominates the baryonic mass content of clusters. But where did it come from and what is the composition of this pervasive ICM? What are the mechanisms that result in the ICM's X-ray luminescence? How do observations of the ICM get converted into physical properties of a cluster? In this section I briefly cover the answers to these questions in order to give the reader a better understanding of the ICM.

Galaxy clusters are built-up during the process of hierarchical merger of dark matter halos and the baryons gravitationally coupled to those halos (White & Rees, 1978). Owing to the inefficiency of galaxy formation and the processes of galactic mass ejection and ram pressure stripping, many of the baryons in these dark matter halos are in the form of diffuse gas and not locked up in galaxies. During the merger of dark matter halos, gravitational potential energy is converted to thermal energy and the diffuse gas is heated to the virial temperature of the cluster potential. The cluster virial temperature is calculated by equating the average kinetic energy of a gas particle to its thermal energy,

$$\frac{1}{2}\mu m\langle\sigma^2\rangle = \frac{3}{2}kT_{virial} \tag{1.1}$$

$$T_{virial} = \frac{\mu m\langle\sigma^2\rangle}{3k} \tag{1.2}$$

where μ is the mean molecular weight, k is the Boltzmann constant, T_{virial} is the virial temperature, m is the mass of a test particle, and $\langle\sigma\rangle$ is the average velocity of the test particle. In this equation, $\langle\sigma\rangle$ can be replaced with the line-of-sight galaxy velocity dispersion (an actual cluster observable) because all objects within the cluster potential (stars, galaxies, protons, ~~kittens)~~ subject to the same dynamics and hence have comparable thermal and kinetic energies. The virial temperature is a fundamental characteristic of a cluster.

Galaxy clusters are the most massive objects presently in the Universe. The enormous mass means deep potential wells and hence very high virial temperatures. Most clusters lie in the temperature range $kT_{virial} = 1-15$ keV. At these energy scales gases are collisionally ionized plasmas and will emit X-rays via thermal Bremsstrahlung. The ICM is not a pure hydrogen gas, as a result atomic line emission will also occur. The ICM is also optically thin at X-ray wavelengths, *e.g.* the optical depth is much smaller than unity, $\tau_\lambda \ll 1$, and hence the X-rays emitted from clusters stream freely into the Universe. I now briefly describe the processes which give rise to ICM X-ray emission and the observables which result. For a magnificently detailed treatise of this topic see Sarazin (1986) and references therein.

1.3.1 X-ray Emission

Detailed study of clusters proceeds mainly through spatial and spectral analysis of the ICM. By directly measuring the X-ray emission of the ICM, quantities such as temperature, density, and luminosity per unit volume can be inferred. Having this knowledge about the ICM provides an observational tool for indirectly measuring ICM dynamics, composition, and mass. In this way a complete picture of a cluster can be built-up and other processes such BCG star formation, AGN feedback activity, or using ICM temperature inhomogeneity to probe cluster dynamic state can be investigated. In this section, I briefly cover how X-ray emission is produced in the ICM and how basic physical properties are then measured.

The main mode of interaction in a fully ionized plasma is the scattering of free electrons off heavy ions. During this process, charged particles are accelerated and thus emit radiation. The mechanism is known as 'free-free' emission (ff), or by the tongue-twisting thermal Bremsstrahlung("braking radiation"). It is also called Bremsstrahlung cooling since the X-ray emission carries away large amounts of energy. The gas particles populating the emitting plasma can be approximated as being

at a uniform temperature with a Maxwell-Boltzmann velocity distribution,

$$f(\vec{v}) = 4\pi \left(\frac{m}{2\pi kT}\right)^{3/2} \vec{v}^2 \exp\left[\frac{-m\vec{v}^2}{2kT}\right] \tag{1.3}$$

where m is mass, T is temperature, k is the Boltzmann constant, and velocity, $\vec{v}$, is defined as $\vec{v} = \sqrt{v_x^2 + v_y^2 + v_z^2}$. The power emitted per cubic centimeter per second from this plasma can be written in the compact form

$$\epsilon_{ff} = 1.4 \times 10^{-27} T^{1/2} n_e n_i Z^2 g_B \tag{1.4}$$

where 1.4×10^{-27} is the condensed form of the physical constants and geometric factors associated with integrating over the power per unit area per unit frequency, n_e and n_i are the electron and ion densities, Z is the number of protons of the bending charge, g_B is the frequency averaged Gaunt factor (of order unity), and T is the global temperature determined from the spectral cut-off frequency. Below the cut-off frequency, $\nu = kT/\hbar$, no photons are created because the energy supplied by charge acceleration is less than the minimum energy required for creation of a photon. Worth noting is that free-free emission is a two-body process and hence the emission goes as the gas density squared while having a weak dependance on the thermal energy, $\epsilon \propto T^{1/2}$.

Superimposed on the thermal emission of the plasma are emission lines of heavy element contaminates such as C, Fe, Mg, N, Ne, O, S, and Si. The widths and relative strengths of these spectral lines are used to constrain the metallicity of the ICM, which is typically quanitified using units relative to Solar abundance, $Z_\odot$. A significant fraction of the ICM, $\sim 0.3Z_\odot$ (Mushotzky & Loewenstein, 1997; Allen & Fabian, 1998b; Fukazawa et al., 1998), is stellar detritus. In collisionally ionized plasmas of the X-ray temperature regime, the dominant ion species is that of the 'closed-shell' helium-like ground state (K and L-shells) [refs]. The K and L shell transitions

are extremely sensitive to temperature and electron densities, therefore providing an excellent diagnostic for constraining both of these quantities. The strongest K-shell transition of the ICM can be seen from iron at $kT \sim 6.7$ keV. If signal-to-noise of the spectrum is of high enough quality, measuring a shift in the energy of this spectral line can be used to confirm or deduce the approximate redshift, and hence distance, of a cluster. The rich series of iron L-shell transitions occur at $0.2 \lesssim T \lesssim 2.0$ keV and are the best diagnostic for measuring metallicity. For the present generation of X-ray instruments, the L-shell lines are seen as a blend with a peak around ~ 1 keV.

Shown in Figs. 1.5 and 1.6 are the unredshifted synthetic spectral models generated with XSPEC (Arnaud, 1996) of a 2 keV and 8 keV gas. Both spectral models have a component added to mimic absorption by gas in the Milky Way (this is seen as attenuation of flux at $E \lesssim 0.4 keV$). For both spectral models the metal abundance is 0.3 $Z_\odot$. These two spectral models differ by only a factor of four in temperature but note the extreme sensitivity of both the thermal Bremsstrahlung exponential cut-off and emission line strengths to temperature.

Equation 1.4 says that observations of ICM X-ray emission will yield two quantities: temperature and density. The gas density can be inferred from the *emission integral*,

$$EI = \int n_e n_p \ dV \qquad (1.5)$$

where n_e is the electron density, n_p is the density of hydrogen-like ions, and dV is the gas volume within a differential element. The emission integral is essentially the sum of the square of gas density for all the gas parcels in a defined region. Thus, the gas density within a projected volume can be obtained from the spectral analysis, but it can also be obtained from spatial analysis of the cluster emission, for example from cluster surface brightness.

The number of photons detected per unit area (projected on the plane of the sky) per second is given the name *surface brightness*. Assuming spherical symmetry,
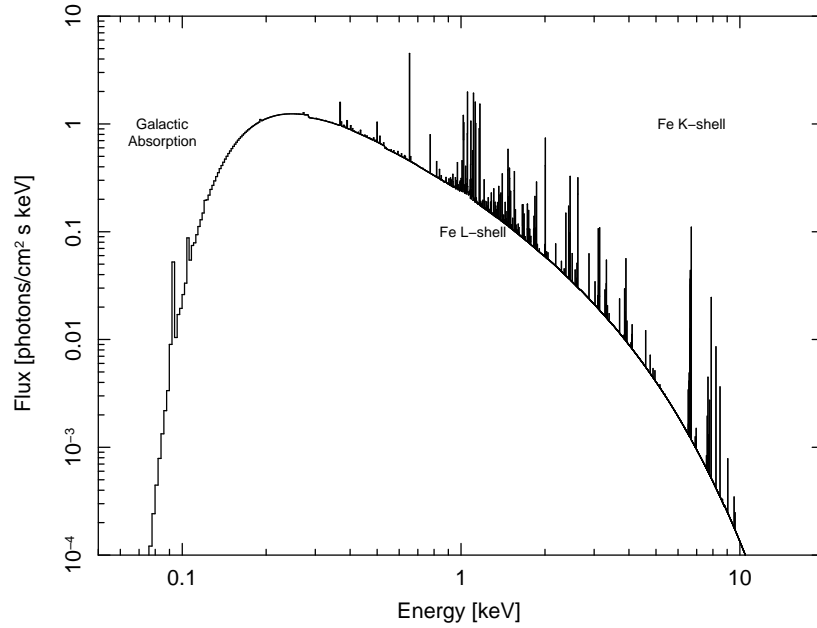
Figure 1.5 Shown here is a synthetic absorbed thermal spectral model of a $N_{HI} = 10^{20}$ cm^{-2}, $kT_X = 2.0$ keV, $Z/Z_\odot = 0.3$, and zero redshift gas. Notice that the strength of the iron L-shell emission lines is much greater than the iron K-shell lines for this model.
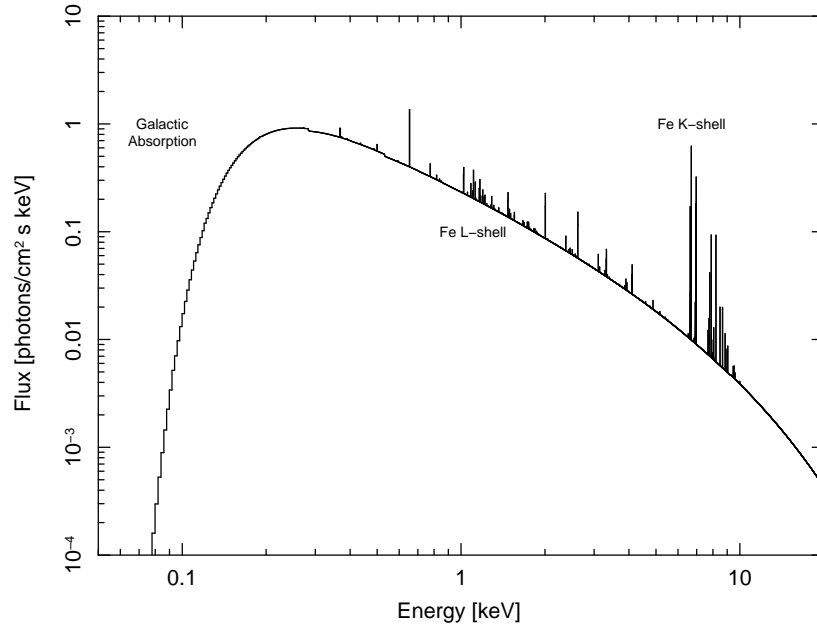
Figure 1.6 Same as Fig. 1.5 except for a $kT_X = 8.0$ keV gas. Notice that for this spectral model the iron L-shell emission lines are much weaker and the iron K-shell lines are mcuh stronger than in the $kT_X = 2.0$ keV model. Also note that the exponential turnover of this model occurs at a higher energy.

2-dimensional surface brightness can be converted to 3-dimensional emission density. By dividing a cluster observation into concentric annuli originating from the cluster center and subtracting off cluster emission at larger radii from emission at smaller radii, the amount of emission from a spherical shell can be reconstructed from the emission in an annular ring. For the spherical shell defined by radii r_i and r_{i+1}, Kriss et al. (1983) shows the relation between the emission density, $C_{i,i+1}$, to the observed surface brightness, $S_{m,m+1}$, of the ring with radii r_m and r_{m+1}, is

$$S_{m,m+1} = \frac{b}{A_{m,m+1}} \sum_{i-1}^{m} C_{i,i+1} \left[(V_{i,m+1} - V_{i+1,m+1}) - (V_{i,m} - V_{i+1,m}) \right]. \quad (1.6)$$

where b is the solid angle subtended on the sky by the object, $A_{m,m+1}$ is the area of the ring, and the V terms are the volumes of various shells. This method of reconstructing the cluster emission is called *deprojection*. While assuming spherical symmetry is clearly imperfect, it is not baseless. The purpose of such an assumption is to attain angular averages of the volume density at various radii from an azimuthally averaged surface density.

In this dissertation the spectral model MeKaL (Mewe et al., 1985, 1986; Liedahl et al., 1995) is used for all of the spectral analysis. The MeKaL model normalization, η, is defined as

$$\eta = \frac{10^{-14}}{4\pi D_A^2 (1+z)^2} \, EI \quad (1.7)$$

where D_A is the angular diameter distance, z is cluster redshift[4], and EI is the emission integral from Eqn. 1.5. Combining Eqns. 1.6 and 1.7 and recognizing that the count rate per volume is equivalent to the emission density, $C_{i,i+1} = cr/\int dV$, yields

---

[4]As is common in all of astronomy, redshift is quantified using the dimensionless ratio of wavelengths: $z = (\lambda_{observed}/\lambda_{rest}) - 1$.

an expression for the electron gas density which is a function of direct observables,

$$n_{\mathrm{e}}(r) = \sqrt{\frac{1.2C(r)\eta(r)4\pi[D_A(1+z)]^2}{f(r)10^{-14}}} \qquad (1.8)$$

where 1.2 is the ionization ratio $n_{\mathrm{e}}=1.2n_{\mathrm{p}}$, $C(r)$ is the radial emission density derived from Eqn. 1.6, η is the spectral normalization from Eqn. 1.7, D_A is the angular diameter distance, z is redshift, and $f(r)$ is the spectroscopic count rate.

Simply by measuring surface brightness and analyzing spectra, the cluster temperature, metallicity, and density can be inferred. These quantities can then be used to derive pressure, $P = nkT$, where $n \approx 2n_{\mathrm{e}}$. The total gas mass can be inferred from $\int (4/3)\pi r^3 n_{\mathrm{e}}$. By further assuming the ICM is in hydrostatic equilibrium, the total cluster mass within radius r is

$$M(r) = \frac{kT(r)}{\mu m G}\left[\frac{d(log\ n_{\mathrm{e}})}{d(log\ r)} + \frac{d(log\ kT)}{d(log\ r)}\right] \qquad (1.9)$$

where all variables have their typical definitions. The rate at which the ICM is cooling can also be expressed in simple terms of density and temperature. Given a cooling function which is sensitive to temperature and metal abundance, $\Lambda(T,Z)$ ($\approx 10^{-23}$ for X-ray temperatures), the cooling rate is $r_{cool} = n^2\Lambda(T,Z)$. For some volume, V, the cooling time is then simply the time required for a gas parcel to radiate away its thermal energy,

$$t_{cool}Vr_{cool} = \frac{3}{2}NkT \qquad (1.10)$$

$$t_{cool} = \frac{\gamma nkT}{2n^2\Lambda(T,Z)} \qquad (1.11)$$

where γ is a constant specific to the type of cooling process (*e.g.* 3/2 for isochoric and 5/2 for isobaric). The cooling time of the ICM can be anywhere between 10^{6-10} yrs. Cooling time has historically been a very important descriptor of the ICM because

processes such as the formation of stars and line-emitting nebulae are sensitive to cooling time.

By simply pointing an X-ray telescope at a cluster and exposing long enough to attain good signal-to-noise it is possible to derive a host of fundamental cluster properties: temperature, density, pressure, mass, cooling time, and even entropy. Entropy is a very interesting quantity which can be calculated using gas temperature and density and is most likely fundamentally connected to processes like AGN feedback and star formation (discussed in Chapters 3 and 4). In the following section I discuss how gas entropy is derived, why it is a useful quantity for understanding clusters, and how it will be utilized later in this dissertation.

1.3.2 Entropy

[NB: This section is woefully lacking of information considering this is a thesis in most part about entropy. I'm in the process of beefing it up.]

The study of ICM entropy has a long history both theoretically and observationally (Bower, 1997; Lloyd-Davies et al., 2000; Tozzi & Norman, 2001; Voit et al., 2002; Pratt et al., 2006; McCarthy et al., 2008). ICM temperature and density alone primarily reflect the shape and depth of the cluster dark matter potential (Voit et al., 2002). But the specific entropy of a gas parcel dictates the density at a given pressure. Thus, properties of the ICM can be viewed as a manifestation of the dark matter potential and the entropy structure. In addition, a gas is convectively stable when $dS/dr \geq 0$, thus without perturbation, the ICM will convect until the lowest entropy gas is near the core and high entropy gas has buoyantly risen to large radii. ICM entropy can also only be changed by addition or subtraction of heat, thus the entropy of the ICM reflects the entire thermal history of the cluster[5]. That a cluster is a huge entropy sorting apparatus and the entropy has recorded the clusters formation and evolution

---

[5]While the reduction of entropy seems to violate the second law of thermodynamics recall that ultimately the Univers is the "isolated" system with which clusters interact.

history will be important for Chapters 3 and 4.

The conventional macroscopic definition of entropy, $dS = dQ/T$ is not that useful in the context of studying astrophysical objects. Thus we must resort to a simpler, measurable surrogate for entropy, like the adiabat. The adiabatic equation of state for a monatomic gas is $P = K\rho^{-\gamma}$ where γ is the ratio of specific heat capacities and has the value of 5/3 for a monatomic gas. Setting $P = \rho kT/\mu m_H$ and solving for K one finds

$$K = \frac{kT}{\mu m_H \rho^{2/3}}.\tag{1.12}$$

where μ is the mean molecular weight of the gas or plasma and m_H is the mass of the Hydrogen atom. The quantity K is refered to as entropy. Although K is called entropy, the true thermodynamic specific entropy is acutally $s = k \ln K^{3/2} + s_0$. A further historical simplification is made to recast K using the simple observables electron density and X-ray temperature: $K = kT/n_e^{2/3}$. With this simple functional form, entropy can now be easily derived from X-ray observations and used to study clusters.

1.4 *Chandra* X-Ray Observatory

In this section I briefly describe what makes the *Chandra* X-ray Observatory (*Chandra* or CXO for short) a groundbreaking and unique telescope ideally suited for the work carried out in this dissertation. In depth details of the telescope, instruments, and spacecraft can be found at the CXO websites[6][7] or in Weisskopf et al. (2000).

The mean free path of an X-ray photon in a gas with the density of the Earth's atmosphere is very short. Oxygen and nitrogen in the atmosphere photoelectrically absorb X-ray photons resulting in 100% attenuation and ~~making~~ X-ray astronomy impossible from the Earth's surface. Many long-standing theories in astrophysics

---

[6]http://chandra.harvard.edu/
[7]http://cxc.harvard.edu/

predict a wide variety of astronomical objects as X-ray emitters. ~~With an obvious need and only one possible solution,~~ astronomers and engineers have been sending X-ray telescopes into the upper atmosphere and space for over 30 years now.

The most recent American X-ray mission to fly is the *Chandra* X-ray Observatory. It is one of NASA's Great Observatories along with *Compton* (γ-rays), *Hubble* (primarily optical), and *Spitzer* (infrared). *Chandra* was built by Northrop-Grumman and is operated by the National Aeronautics and Space Agency. *Chandra* was launched in July 1999 and resides in a highly elliptical orbit with an apogee of $\sim 140,000$ km and a perogee of $\sim 16,000$ km. One orbit takes ≈ 64 hours to complete. The telescope has four nested Iridium coated parabaloid-hyperboloid mirrors with a focal length of ~ 10 m.

All data presented in this dissertation was collected with the Advanced CCD Imaging Spectrometer (ACIS) instrument[8]. ACIS is quite an amazing and unique instrument in that it is an imager and medium-resolution spectrometer at the same time. When an observation is taken with ACIS, the data collected contains spatial and spectral information since the location and energy of incoming photons are recorded. The dual nature of ACIS allows the data to be analyzed by spatially dividing up a cluster image and then extracting spectra for these subregions of the image, a technique which is used heavily in this dissertation.

The observing elements of ACIS are 10 1024×1024 CCDs: six linearly arranged CCDs (ACIS-S array) and four CCDs arranged in a 2×2 mosaic (ACIS-I array). The ACIS focal plane is currently kept at a temperature of ~ -120 °C. A pre-launch photograph of ACIS is shown in Fig. 1.7. During an observation the spacecraft is dithered along a Lissajous curve so parts of the sky which fall in the chip gaps are also observed. Dithering also ensures pixel variations of the CCD response are removed.

The high spatial and energy resolution of *Chandra* and its instruments are ideal for

---

[8]http://acis.mit.edu/acis
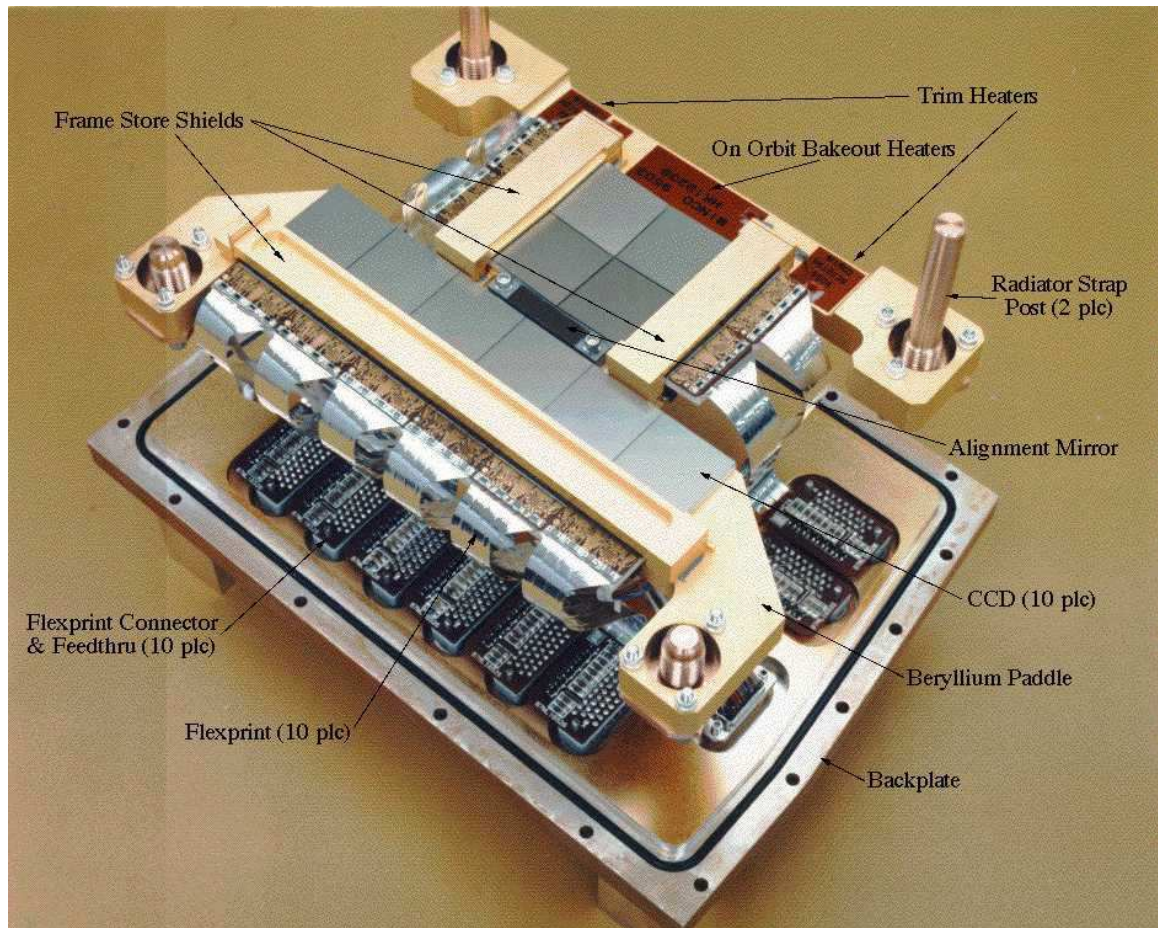
Figure 1.7 This is a pre-launch photograph of the ACIS instrument. The S-array is the line of six CCDs (gray squares) atop the Beryllium Paddle, and the I-array is the mosaic of four CCDs near the On-Orbit Bakeout Heaters. Image taken from Chandra X-ray Center. Per NASA copyright policy: "NASA material is not protected by copyright unless noted".

studying clusters of galaxies. The telescope onboard *Chandra* achieves on-axis spatial resolutions of $\lesssim 0.5''$/pixel but it is the pixel size of the ACIS instrument ($\sim 0.492''$) which sets the resolution limit for observations. ACIS also has an extraordinary energy resolution of $\Delta E/E \sim 100$. Below energies of ~ 0.3 keV and above energies of ~ 10 keV the ACIS effective area is ostensibly zero. The ACIS effective area also peaks in the energy range $E \sim 0.7 - 2.0$ keV. As shown in Figs. 1.5 and 1.6, a sizeable portion of galaxy cluster emission occurs in the same energy range where the ACIS effective area peaks. The energy resolution of ACIS also allows individual emission line blends to be resolved in cluster spectra. These aspects make *Chandra* a perfect choice for studying clusters and the ICM in detail. Shown in Fig. 1.8 are raw observations of Abell 1795 with the aimpoints on ACIS-I (top panel) and ACIS-S (bottom panel). In Fig. 1.9 is a spectrum for the entire cluster extracted from the ACIS-I observation.
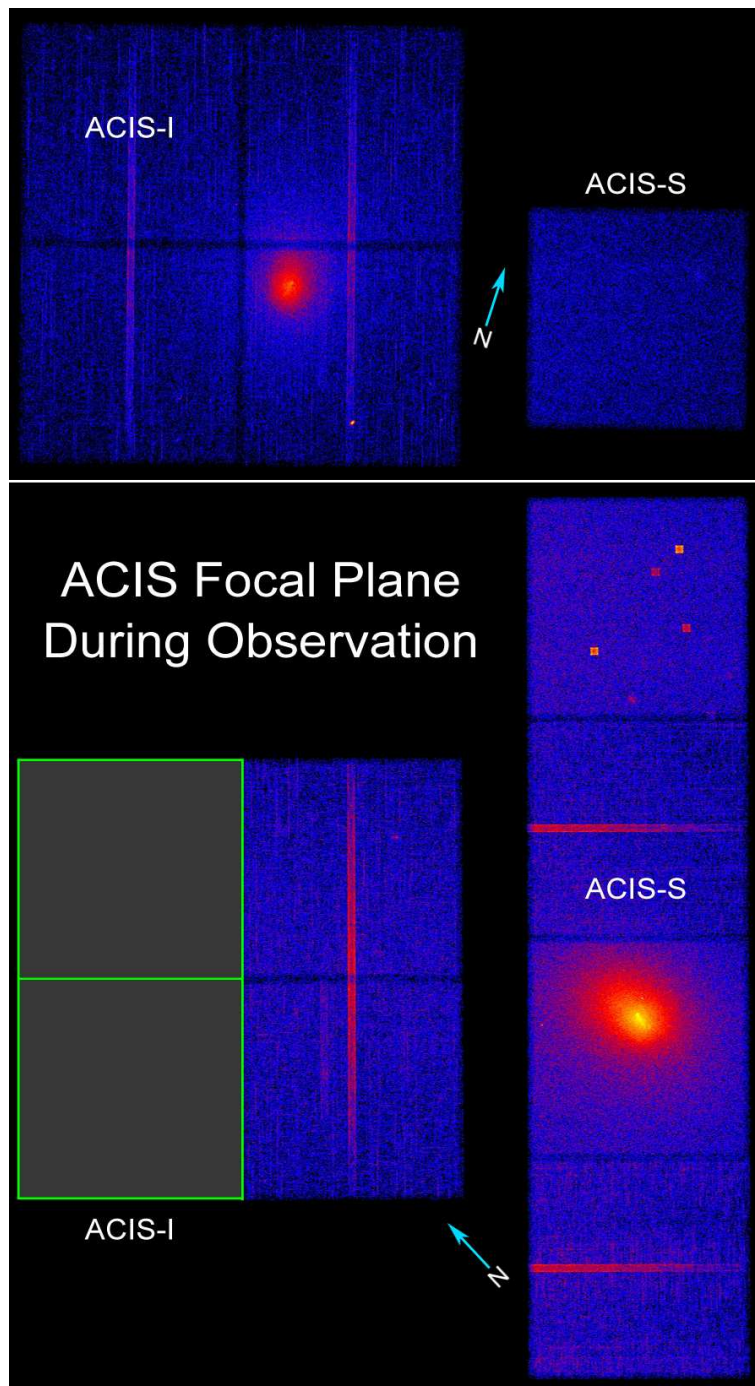
Figure 1.8 In both panels celestial North is indicated by the blue arrow. *Top panel:* ACIS-I aimed observation of Abell 1795. The image has been binned by a factor of four so the whole field could be shown. *Bottom panel:* ACIS-S aimed observation of Abell 1795. Again, the image is binned by a factor of four to show the whole field. For reference, the green boxes mark the ACIS-I chips which were off during this observation.
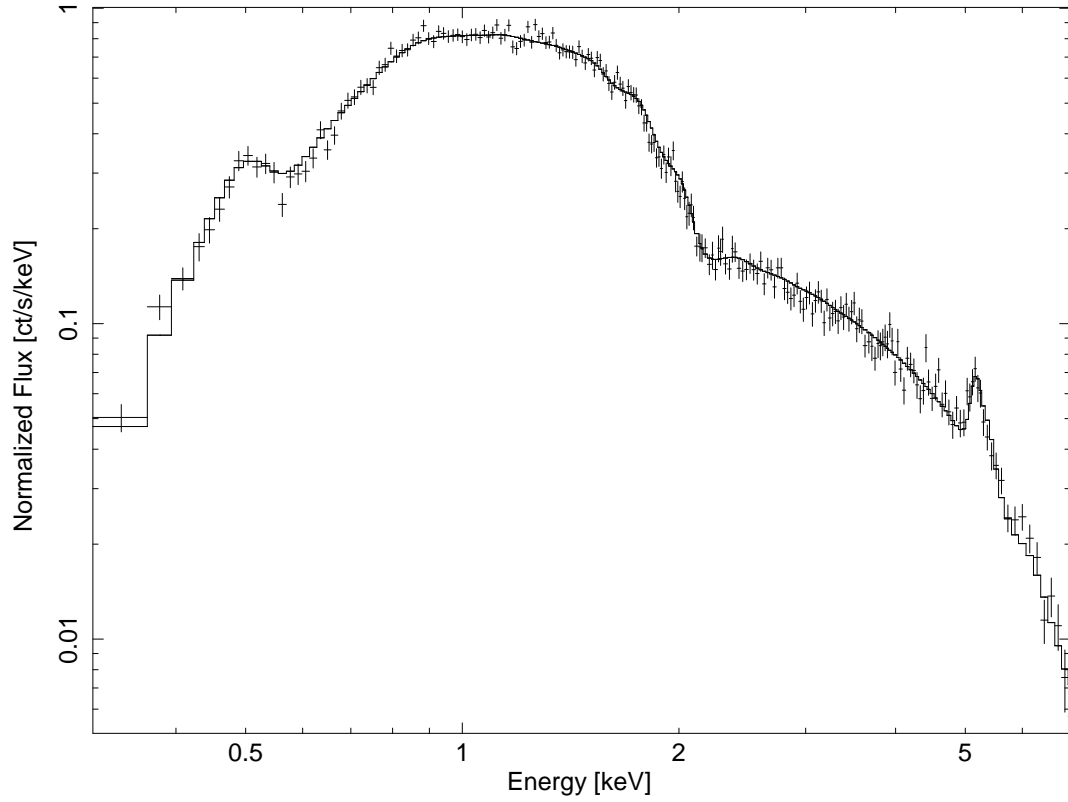
Figure 1.9 Global spectrum of the cluster Abell 1795 with the best-fit single-component absorbed thermal spectral model overplotted (solid line). Comparing this spectrum with those of Figs. 1.5 and 1.6, the effects of finite energy resolution and convolving the spectral model with instrument responses are apparent. Individual spectral lines are now blends and the spectral shape for $E < 1.0$ has changed because of diminishing effective area.

CHAPTER 2:
ENERGY BAND DEPENDENCE OF
X-RAY TEMPERATURES

CHAPTER 3:
CHANDRA ARCHIVAL SAMPLE OF INTRACLUSTER ENTROPY PROFILES

CHAPTER 4:
AN ENTROPY THRESHOLD FOR STRONG Hα AND RADIO EMISSION IN THE CORES OF GALAXY CLUSTERS

CHAPTER 5:
SUMMARY

5.1 SUMMARY OF CHAPTERS

5.1.1 ENERGY BAND DEPENDENCE OF X-RAY TEMPERATURES

5.1.2 CHANDRA ARCHIVAL SAMPLE OF INTRACLUSTER ENTROPY PROFILES

5.1.3 AN ENTROPY THRESHOLD FOR STRONG Hα AND RADIO EMISSION IN THE CORES OF GALAXY CLUSTERS

5.2 FUTURE WORK

BIBLIOGRAPHY

REFERENCES

Alexander, P. 2002, MNRAS, 335, 610

Allen, S. W., & Fabian, A. C. 1998a, MNRAS, 297, L57

—. 1998b, MNRAS, 297, L63

Arnaud, K. A. 1996, in ASP Conf. Ser. 101: Astronomical Data Analysis Software and Systems V, ed. G. H. Jacoby & J. Barnes, 17–+

Arnaud, M., & Evrard, A. E. 1999, MNRAS, 305, 631

Bialek, J. J., Evrard, A. E., & Mohr, J. J. 2001, ApJ, 555, 597

Borgani, S., Governato, F., Wadsley, J., Menci, N., Tozzi, P., Quinn, T., Stadel, J., & Lake, G. 2002, MNRAS, 336, 409

Borgani, S., Rosati, P., Tozzi, P., Stanford, S. A., Eisenhardt, P. R., Lidman, C., Holden, B., Della Ceca, R., Norman, C., & Squires, G. 2001, ApJ, 561, 13

Bower, R. G. 1997, MNRAS, 288, 355

Bower, R. G., Benson, A. J., Lacey, C. G., Baugh, C. M., Cole, S., & Frenk, C. S. 2001, MNRAS, 325, 497

Brüggen, M., & Kaiser, C. R. 2002, Nature, 418, 301

Brüggen, M., Kaiser, C. R., Churazov, E., & Enßlin, T. A. 2002, MNRAS, 331, 545

Bryan, G. L., & Norman, M. L. 1998, ApJ, 495, 80

Cavaliere, A., Menci, N., & Tozzi, P. 1999, MNRAS, 308, 599

Churazov, E., Sunyaev, R., Forman, W., & Böhringer, H. 2002, MNRAS, 332, 729

Clowe, D., Bradač, M., Gonzalez, A. H., Markevitch, M., Randall, S. W., Jones, C., & Zaritsky, D. 2006, ApJ, 648, L109

Dalla Vecchia, C., Bower, R. G., Theuns, T., Balogh, M. L., Mazzotta, P., & Frenk, C. S. 2004, MNRAS, 355, 995

Donahue, M., Horner, D. J., Cavagnolo, K. W., & Voit, G. M. 2006, ApJ, 643, 730

Donahue, M., Sun, M., O'Dea, C. P., Voit, G. M., & Cavagnolo, K. W. 2007, AJ, 134, 14

Edge, A. C., & Stewart, G. C. 1991, MNRAS, 252, 414

Evrard, A. E., & Henry, J. P. 1991, ApJ, 383, 95

Evrard, A. E., Metzler, C. A., & Navarro, J. F. 1996, ApJ, 469, 494

Fabian, A. C. 1994, ARA&A, 32, 277

Finoguenov, A., Reiprich, T. H., & Böhringer, H. 2001, A&A, 368, 749

Fukazawa, Y., Makishima, K., Tamura, T., Ezawa, H., Xu, H., Ikebe, Y., Kikuchi, K., & Ohashi, T. 1998, PASJ, 50, 187

Hoeft, M., & Brüggen, M. 2004, ApJ, 617, 896

Jeltema, T. E., Hallman, E. J., Burns, J. O., & Motl, P. M. 2007, ArXiv e-prints, 708

Kaiser, N. 1986, MNRAS, 222, 323

—. 1991, ApJ, 383, 104

Kalberla, P. M. W., Burton, W. B., Hartmann, D., Arnal, E. M., Bajaja, E., Morras, R., & Pöppel, W. G. L. 2005, A&A, 440, 775

Krauss, L. M., & Scherrer, R. J. 2007, General Relativity and Gravitation, 39, 1545

Kriss, G. A., Cioffi, D. F., & Canizares, C. R. 1983, ApJ, 272, 439

Liedahl, D. A., Osterheld, A. L., & Goldstein, W. H. 1995, ApJ, 438, L115

Lloyd-Davies, E. J., Ponman, T. J., & Cannon, D. B. 2000, MNRAS, 315, 689

Markevitch, M., Gonzalez, A. H., David, L., Vikhlinin, A., Murray, S., Forman, W., Jones, C., & Tucker, W. 2002, ApJ, 567, L27

Markevitch, M., & Vikhlinin, A. 2007, Phys. Rep., 443, 1

McCarthy, I. G., Babul, A., Bower, R. G., & Balogh, M. L. 2008, MNRAS, 386, 1309

McCarthy, I. G., Balogh, M. L., Babul, A., Poole, G. B., & Horner, D. J. 2004, ApJ, 613, 811

McDonough, W., & Braungart, M. 2002, Cradle to Cradle: Remaking the Way We Make Things (New York: North Point Press)

McNamara, B. R., & Nulsen, P. E. J. 2007, ARA&A, 45, 117

Mewe, R., Gronenschild, E. H. B. M., & van den Oord, G. H. J. 1985, A&AS, 62, 197

Mewe, R., Lemen, J. R., & van den Oord, G. H. J. 1986, A&AS, 65, 511

Mohr, J. J., Mathiesen, B., & Evrard, A. E. 1999, ApJ, 517, 627

Mushotzky, R. F. 1984, Physica Scripta Volume T, 7, 157

Mushotzky, R. F., & Loewenstein, M. 1997, ApJ, 481, L63+

Omma, H., Binney, J., Bryan, G., & Slyz, A. 2004, MNRAS, 348, 1105

Peterson, J. R., & Fabian, A. C. 2006, Phys. Rep., 427, 1

Peterson, J. R., Paerels, F. B. S., Kaastra, J. S., Arnaud, M., Reiprich, T. H., Fabian,
A. C., Mushotzky, R. F., Jernigan, J. G., & Sakelliou, I. 2001, A&A, 365, L104

Pizzolato, F., & Soker, N. 2005, ApJ, 632, 821

Pratt, G. W., Arnaud, M., & Pointecouteau, E. 2006, A&A, 446, 429

Riess, A. G., Filippenko, A. V., Challis, P., Clocchiatti, A., Diercks, A., Garnavich,
P. M., Gilliland, R. L., Hogan, C. J., Jha, S., Kirshner, R. P., Leibundgut, B.,
Phillips, M. M., Reiss, D., Schmidt, B. P., Schommer, R. A., Smith, R. C., Spy-
romilio, J., Stubbs, C., Suntzeff, N. B., & Tonry, J. 1998, AJ, 116, 1009

Riess, A. G., Strolger, L.-G., Casertano, S., Ferguson, H. C., Mobasher, B., Gold, B.,
Challis, P. J., Filippenko, A. V., Jha, S., Li, W., Tonry, J., Foley, R., Kirshner,
R. P., Dickinson, M., MacDonald, E., Eisenstein, D., Livio, M., Younger, J., Xu,
C., Dahlén, T., & Stern, D. 2007, ApJ, 659, 98

Roychowdhury, S., Ruszkowski, M., Nath, B. B., & Begelman, M. C. 2004, ApJ, 615,
681

Ruszkowski, M., & Begelman, M. C. 2002, ApJ, 581, 223

Sarazin, C. L. 1986, Reviews of Modern Physics, 58, 1

Sharpee, B., Zhang, Y., Williams, R., Pellegrini, E., Cavagnolo, K., Baldwin, J. A.,
Phillips, M., & Liu, X.-W. 2007, ApJ, 659, 1265

Soker, N., & Pizzolato, F. 2005, ApJ, 622, 847

Tamura, T., Kaastra, J. S., Peterson, J. R., Paerels, F. B. S., Mittaz, J. P. D.,
Trudolyubov, S. P., Stewart, G., Fabian, A. C., Mushotzky, R. F., Lumb, D. H., &
Ikebe, Y. 2001, A&A, 365, L87

Thomas, P. A., Fabian, A. C., & Nulsen, P. E. J. 1987, MNRAS, 228, 973

Tozzi, P., & Norman, C. 2001, ApJ, 546, 63

Ventimiglia, D., Voit, G. M., Borgani, S., & Donahue, M. 2008, ApJ Submitted

Voit, G. M. 2005, Reviews of Modern Physics, 77, 207

Voit, G. M., & Bryan, G. L. 2001, Nature, 414, 425

Voit, G. M., Bryan, G. L., Balogh, M. L., & Bower, R. G. 2002, ApJ, 576, 601

Voit, G. M., Cavagnolo, K. W., Donahue, M., Rafferty, D. A., McNamara, B. R., & Nulsen, P. E. J. 2008, ArXiv e-prints, arxiv:0806.0384

Voit, G. M., & Donahue, M. 2005, ApJ, 634, 955

Weisskopf, M. C., Tananbaum, H. D., Van Speybroeck, L. P., & O'Dell, S. L. 2000, in Presented at the Society of Photo-Optical Instrumentation Engineers (SPIE) Conference, Vol. 4012, Proc. SPIE Vol. 4012, p. 2-16, X-Ray Optics, Instruments, and Missions III, Joachim E. Truemper; Bernd Aschenbach; Eds., ed. J. E. Truemper & B. Aschenbach, 2–16

White, S. D. M., Efstathiou, G., & Frenk, C. S. 1993, MNRAS, 262, 1023

White, S. D. M., & Rees, M. J. 1978, MNRAS, 183, 341

APPENDICES

Appendix A:
Chandra Observations Reduction Pipeline (CORP)

This appendix has been written as a tutorial for the first-time analyzer of *Chandra* data (*e.g.* the "you" role in the text).

A.1 Introduction to CORP

The reduction and analysis of *Chandra* data is given in exquisite detail in the CIAO threads on the CXC's website[1]. There is very little which is not discussed in the CIAO and HelpDesk threads at the CXC website. However, to streamline the lengthy reduction and analysis process of extended X-ray sources, such as galaxy clusters and groups, I have written several PERL and IDL scripts which make-up my own *Chandra* Observations Reduction Pipeline (CORP, pronounced "core"). The purpose of this pipeline software is to condense CIAO's tedious prompts and command line intensive steps into an easily executable series of scripts which require minimal interaction and produce science-ready data products. A pipeline also ensures that a large sample of observations are reduced the same way, and a pipeline also eases the pain of analyzing several hundred observations.

There is a critical caveat to the use of CORP and analyzing *Chandra* data in general: **no two *Chandra* observations are the same!** CORP has allowances

---

[1]http://cxc.harvard.edu/ciao/threads/index.html

for many different tool settings and instrument setups, but these options are finite, and no amount of automation can replace human interactivity. It is an absolute **necessity** that users of CORP view, scrutinize, and double check the output of every reduction/analysis step. This can be time consuming, but not nearly as time consuming as finding and correcting errors embedded in on-going, or goodness forbid, **published** work.

As of writing this dissertation, all CORP scripts properly interact with CIAO 3.4.1 and CALDB 3.4. The CXC software versions matter because the CXC programmers (whom are great people!) have a tendency to reinvent the wheel every so often. This may result in a change to output filenames, extensions, header keywords, data types, et cetera and can cause a script to err. Errors are not guaranteed however, so it is important to be mindful of how CIAO or the CALDB have changed as a result of an update (release notes are always provided with an update: read them!). There are some pretty great updates to CIAO included in the full, final 4.0 version, so I highly recommend CORP users email me to request new scripts when CIAO 4.0 is fully deployed.

Now for a few notes about me, the author and programmer:

1. I use plenty of analysis and X-ray "jargon" in this Appendix. If you come across nomenclature which is unfamiliar, consult the CXC website, there is absolutely nothing you could want to know about *Chandra* that is not there. CORP is my method for automating most of the logic trees which are in the CXC threads, but this does not mean CORP's operation will always be transparent to a user.

2. I am not a computer programmer. In fact, I only knew psuedo-code when I entered graduate school. Hence, my style of programming is best described as unelegant and brutish. Computer resources are cheap and abundant, so I use lots of ineffcent code, but the overhead and time consumption are low, so writing efficient code does nothing to accelerate my work. The scripts of CORP

use no command line options besides input, and sometimes output, filenames. Everything the script is being commanded to do is controlled by opening the code and editing the "Options" section near the beginning of the program. Do not worry, it's as simple as editing a Word document.

3. As of now, the scripts are available via a tarball which I will email you. Someday distribution of the code will be handled through a public CVS server. The tarball contains all the scripts, a README file (which is a copy of this appendix), and a folder of example data. Descriptions of what each script does, how it is called, what it takes as input, and what is generated as output are all listed in the header of each program.

4. I am not a debugger. Each script is written to run a very specific set of tasks. Given the proper input, the scripts return the expected output. However, while I wish the scripts were magic, alas, they are not. If you plan on giving the programs non-standard input and there is some operation you are not sure the script will perform, then find out first by dissecting the code. I may have coded a script to handle your odd data, but I may not. Find out first!

A.2   COPYRIGHT

As a formality, I have blanketed CORP with the GNU General Public License. Below is the copyright and license agreement for all scripts in CORP:

Kenneth W. Cavagnolo's Chandra Observations Reduction Pipeline (CORP)

Copyright © 2008 Kenneth W. Cavagnolo, `kencavagnolo@gmail.com`

These programs are free software; you can redistribute them and/or modify them under the terms of the GNU General Public License as published by the Free Software Foundation; either version 2 of the License, or (at your option) any later version. These programs are distributed in the hope that they will be useful, but WITHOUT

ANY WARRANTY; without even the implied warranty of MERCHANTABILITY or FITNESS FOR A PARTICULAR PURPOSE. See the GNU General Public License for more details. You should have received a copy of the GNU General Public License along with these programs; if not, write to the Free Software Foundation, Inc., 51 Franklin Street, Fifth Floor, Boston, MA 02110-1301, USA.

A.3   RETRIEVING DATA

"When your CIAO-Fu is good, only then will you utilize the stowed backgrounds of the CALDB."

Getting *Chandra* data from the CDA is not complicated. There are two methods to get data: 1) run the stand-alone *Chaser* program, or 2) use the web-based version of *Chaser*, named *WebChaser*, at http://cda.harvard.edu/chaser/. I have found that the download speeds via *Chaser* are much slower than those achieved with *WebChaser*, and hence I highly suggest using *WebChaser*. The *WebChaser* form is self-explanatory: enter either an object name, right ascension (R.A.) and declination (Decl.) of an object, use the object name to find R.A. and Decl. (providing the name you give is listed in NED or Simbad), or any other number of search methods.

After searching the CDA for what you want, a list of archived observations will be returned. **VERY IMPORTANT:** Now is the time to make a one column file where each line lists one of the ObsIDs to be downloaded:

```
#Obsid
2419
791
etc.
```

This file will be used in the first step of CORP and you will be miserable if you don't do this now. Now, click the "Select All" link, followed by the "Add to Retrieval

List" button, then click the "Retrieve Products" button, and after the CDA disks are queued an FTP address will be given to download the tarball of files. From here just download the file via Firefox, Cyberduck, or use the fastest method, `wget`. With the tarball downloaded, simply unpack it in a location where you're keeping data:

```
[linux]% wget ftp://<ftp_address_from_chaser>/package.tar
[linux]% cd <hard_drive>/<my_root_datadir>/
[linux]% tar -xvf <path_tarball>/package.tar
```

You will now have new directories which bear the names of the downloaded ObsIDs (for example, `<hard_drive>/<my_root_datadir>/<obsid>`).

Great! The data is now out of the archive and into your hands. What are all these different files? The answer to that question is lengthy and of fundamental importance in honing your CIAO-Fu. Read the documentation on data products at the following webpages:

http://cxc.harvard.edu/ciao/data/basics.html

http://cxc.harvard.edu/ciao/threads/intro_data/

A.4   INITIAL REPROCESSING

A.4.1   GENERATE REFERENCE LIST

If you have downloaded and unpacked the data, know why the `PCAD` files are so important and why nothing matters without `evt` files, then now is the time to start using CORP. At the heart of most CORP scripts is an input reference file. The reference file is a listing of all the ObsIDs you want to analyze and also contains details about each cluster associated with each ObsID. Recall the one column file of ObsIDs? This file will now used in conjunction with `query_cda.pl` to create the reference file. In the script `query_cda.pl` there are two options, `$get_nh, $get_z`, which when set to 'yes' tell the script to find the Galactic absorbing column density

(N_{HI}) from the LAB survey (Kalberla et al., 2005) and redshift from NED[2]. The `$get_nh` is trustworthy, so set it to 'yes'. However, the `$get_z` option is not robust. The NED query returns a list of galaxy clusters nearest the aimpoint of the *Chandra* observation, but the proper redshift is not always returned. I typically leave this option set to 'yes' and confirm redshifts by manually querying NED (hey, it's less typing). Now run the script (**WARNING:** If there is an existing `newref.list` in the working directory, it will be overwritten):

```
[linux]% perl query_cda.pl <my_list_of_obsids>
```

The script tells the user what N_{HI} and redshift it has found and for what object. The script also informs the user how many of the input ObsIDs were successfully found in the CDA and the total exposure time of observations in the query.

There should now be a new file named `newref.list`. Each column of `newref.list` is described below:

Name: This is the name of the `TARGET` object listed for the observation. This is not necessarily the name you'd like to give the object, so feel free to change it.

ObsID: Obviously this is the ObsID. Most of the file naming convention in CORP involves the ObsID since it is a unique identifier. This may seem clumsy and awkward (especially for the clusters that have multiple ObsIDs) but in the battle of clarity and brevity, clarity wins in my book.

RA: The right ascension of the observation target object. The default output format is decimal degrees, but this can be changed to sexigesimal by changing the `query_cda.pl` variable `$outcrdunit` from 'decimal' to 'sexigesimal'.

Dec: The declination of the observation target object in decimal degrees.

Rmax: The maximum observation radius. This is the radius from the cluster center to the nearest detector edge. Rmax needs to be specified by the user for each observation. A script which automatically finds Rmax is forthcoming.

---

[2]http://nedwww.ipac.caltech.edu/

MinCts: The minimum number of counts per temperature annulus. The default is 2500 but this number should be increased for observations with sufficient counts or adjusted depending on scientific goals.

z: The redshift of the target object. Even if the script has automatically queried NED for this value, it is best to double-check. A batch query via NED is easy following the directions at http://nedwww.ipac.caltech.edu/help/batch.html.

Nh20: The galactic absorbing neutral hydrogen column density, N_{HI}, in 10^{20} cm^{-2}. These values are acquired from the `nh` tool which uses the L.A.B. Survey results (Kalberla et al., 2005).

Tx: The global/virial cluster temperature. There are a number of ways to measure to a cluster temperature, it is best to keep a detailed record of how you made this measurement or where you looked-up the temperature (*e.g.* KEEP CITATIONS you'll want them later).

Fe: The global cluster metallicity. The value listed in the reference file is used only as a starting point for most spectral fits, so the value listed is not all that important. I'd go as far to say this is a depricated entry. Again, if this value if looked-up in the literature, keep a citation record.

Lbol: The cluster bolometric luminosity. *Chandra* has a small field of view, so if this is a value best taken from the literature, for example from Horner's dissertation[3].

Chip: The CCD on which the cluster center is located. The default is to list the array on which the observation is taken (I or S), but specifying which `chip_id` (*i.e.* S3 or I0) is left to the user.

E_obs, Diff, Robs: These are depricated columns which have been left-in because most scripts were written before they were no longer needed. Forthcoming versions of CORP will not need these columns.

---

[3]http://asd.gsfc.nasa.gov/Donald.Horner/thesis.html

Location: Sometimes data is stored across multiple volumes, hence this column specifies the path to each ObsID. For example if one ObsID is stored on `/mnt/HD1` and another is on `/media/USB1`. This allows a single instance of a script to be run on distributed data.

Included in the CORP tarball is a script named `ds9_viewreg.pl`. The script is very useful for viewing observations quickly and has been invaluable throughout the years. The program performs a multitude of tasks and relies on the functionality of DS9[4]. The script header completely explains all the variables and how to use the program. Before starting the bulk of data reduction I recommend using `ds9_viewreg.pl` to determine the Chip and Rmax values for each ObsID and then entering them into the `newref.list` file.

A.4.2 CREATE NEW LEVEL-2 EVENTS FILE

Before completing any true analysis, such as finding the cluster center or identifying point sources, the CIAO threads recommend creating a new events file. Removing bad grades, time intervals with flares, bad pixels, et cetera ensures that analysis further downstream is more robust. The initial reprocessing step described here requires running the script `reprocess.pl` with some, but not all, of the internal switches set to "yes". Descriptions for the internal switches of this program are in the code header. The program `reprocess.pl` performs multiple tasks and will be used more than once: In the first pass, `reprocess.pl` will perform the tasks outlined below, later it will be used to exclude point sources. For more detail on any of the steps below, read:

http://cxc.harvard.edu/ciao/guides/acis_data.html

http://cxc.harvard.edu/ciao/threads/createL2/.

First, edit the script so all the options are "yes" and only `$exclude` is equal to

---

[4]http://hea-www.harvard.edu/RD/ds9/

"no". To run the script, simply call it with perl giving the reference file as input (if you do not want an ObsID analyzed, simply comment it out of the reference file by placing a "#" at the front of the line):

```
[linux]% perl reprocess.pl reference.list
```

For each ObsID in the reference file, a new `reprocessed` subdirectory has been created and all new files have been placed in that directory. The output files are listed at the end of the script header. The reduction steps performed by `reprocess.pl` are: remove the ACIS afterglow, create a new bad pixel file, set `ardlib.par`, update time-dependent gain (TGAIN), apply charge tranfer inefficency (CTI) correction (if appropriate), filter on event grade, filter on good time intervals (GTIs), destreak, remove background flares and/or periods of excessively high background, make blank-sky background file, and make off-axis blank-sky background file.

Cleaning for flares is a detailed step and is best understood by reading the CIAO documentation. The main steps in extracting and filtering a light curve are removing bright sources, setting the time bin size specific to front or back illuminated CCDs, setting the energy window for the specific CCD type, analyzing the light curve using the contributed routine `lc_clean.sl`, and filtering out the time periods from the GTIs which contain high background. All of these steps are handled automatically by the script, however `lc_clean.sl` **DOES NOT** always find the proper background count rate mean. This results in the beginning or end of flare not being excluded from the GTIs, while perfectly good intervals are excluded (see Figure A.1 as an example). The solution to this problem is very simple.

After reprocessing you should examine each light curve anyway, so finding these cases will be easy. Run the script `view_prof.pl` with the internal switches set to view lightcurves. When you find a case where a flare has been improperly removed, estimate the mean background count rate by finding the peak in the count rate distribution in the bottom pane of the figure. Now we'll create a new ASCII file

which contains information about this OBSID and it's flare. The file should have the format:

```
#Obsid  Mean Rate
2419    1.300
791     0.175
```

Save this file, set the `$flarefile` keyword in `reprocess.pl` to point to this new file, and now re-run `reprocess.pl` with all other options set to "no" except the `$clean_events` option which should be "yes". Examine the new lightcurve and repeat this process if the mean is not exactly where you think it should be.

Making blank-sky backgrounds is easily the most involved step in `reprocess.pl` and to fully understand what is being done, reading Maxim Markevitch's Cookbook[5] in conjunction with the background thread[6] are a must.

After `reprocess.pl` has finished running, it is wise to spend the time examining all of the output files. This entails steps such as viewing the `evt1`, `evt2`, `bgevt`, and `clean` files; checking the light curves for missed or inproperly excluded flares; verifying the background file have the proper exposure times in the headers. If the data is trustworthy, then move along.

A.4.3 REMOVE POINT SOURCES AND IDENTIFY CLUSTER CENTER

Determining the cluster center and identifying points sources for exclusion is a crucial step in extended source analysis as these steps significantly affect the final results. Reliably determing the cluster center and finding point sources first requires an exposure map. An exposure map is a replication of the optical system's characteristics (*e.g.* CCD quantum efficiency, CCD non-uniformities, vignetting, bad pixels, etc.) dithered and exposed exactly as the observation. The exposure map is used to re-

---

[5]http://cxc.harvard.edu/contrib/maxim/acisbg/
[6]http://cxc.harvard.edu/ciao/threads/acisbackground/

Lightcurve: 897_lc.fits
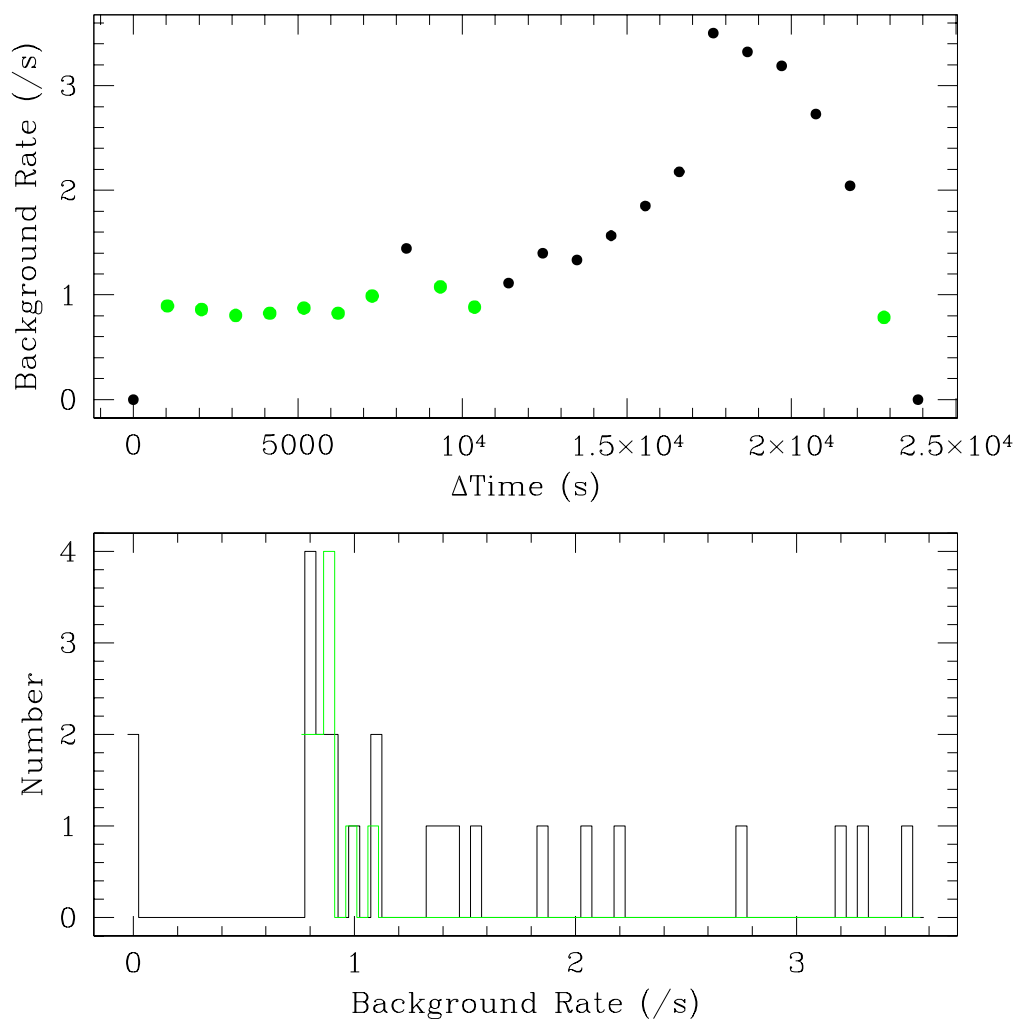
Figure A.1 Shown here is an example light curve output by `lc_clean.sl` which is called when `reprocess.pl` is run. *Top panel:* Plot of background count rate versus time in the observation. Green points mark those time intervals within $\pm20\%$ of the mean rate. Zero rate bins at the beginning and end of an observation are intentional dead times. The flares can easily be identified in this example. Also note that the automated mean detection did not remove the wings at ~ 5 ksec and ~ 9 ksec of the weaker flare. *Bottom panel:* Histogram of the light curve shown in the top panel. The green line is again for the intervals within $\pm20\%$ of the mean rate.

move instrumental features, like chip gaps, which will be erroneously detected as point sources or skew the calculation of the cluster center.

There are two ways of calculating an exposure map: using a monoenergetic incident spectrum or a more specific spectral model. The script for making exposure maps can do both, and it is up to the user to determine if one or the other is preferred for their analysis. For all of the clusters I have analyzed, the monoenergetic assumption does not give significantly different results from the more elegant spectral model method.

There are many options for making an exposure map and they are explained in the script header. To make an exposure map, run the script `exp_map.pl`:

```
[linux]% perl exp_map.pl reference.list
```

The output will be an instrument map, aspect histogram, exposure map, and a normalized image of the cluster (in flux units). The normalized image is what will be used to find point sources and find the cluster center. By default, the script makes a full resolution (binning=1) exposure map. This has the drawback of being time consuming, but the advantage of more accuracy in spatial analysis. If you are simply experimenting data, then increase the binning factor to four or eight. I do not recommend using such highly binned data for analysis unless the cluster center is especially obivous (*i.e.* in highly peaked clusters) or you plan on remaking point source exclusion regions by hand.

Now that you have an exposure map, edit the options in the script `cent_emi.pl` and run the script.

```
[linux]% perl cent_emi.pl reference.list
```

or

```
[linux]% perl dub_centroid.pl dub_reference.list
```

This program will find the cluster centroid and peak using the CIAO tool `dmstat`. If these two quantities differ by less than 70 kpc, the peak will be returned as the

cluster center. The script also outputs a new reference file with the cluster center in the RA and Dec columns. Now is the moment to be a researcher: view the clusters with the center marked, does this solution look right?

After determining if the cluster center finder worked properly, the next step is to identify and exclude point sources. The script which does this is `find_pt_src.pl` which calls the CIAO tool `wavdetect`. The primary script output is an ASCII file listing the exclusion regions.

```
[linux]% perl find_pt_src.pl reference.list
```

It is very important at this stage to view the observation with the exclusion regions overlaid. The `wavdetect` algorithm is very sophisticated, however it will miss sources (*e.g.* sources very close together), detect spurious sources (*e.g.* chip gaps and edges), detect sources which are bright, diffuse cluster emission (*e.g.* the core of a bright, peaky cluster), and miss sources in regions of high background (*e.g.* point sources in or near bright cluster core).

While viewing the observation and regions with `ds9_viewreg.pl`, it is straight forward to delete, add, and alter regions. After doing so, go to the 'Regions' menu, 'File Format' tab, and click 'Ciao'. Then under the 'Regions' menu click 'Save regions...' and simply overwrite the loaded `<obsid>_exclude.reg` region file. That is all it takes to edit the exclusion regions in a quick, by-eye batch session. Now edit the script `reprocess.pl` so that all options are "no" except for the `$exclude` option which should be "yes". Running `reprocess.pl` will now remove all the regions you just saw/specified in DS9.

```
[linux]% perl reprocess.pl reference.list
```

The output from this final step is the file `<obsid>_exclude.fits` which is the crown jewel of CORP: an up-to-date, flare-clean, point source-clean, events file at level-2. As usual, you should view this file and make sure the point source exclusion functioned as expected. The initial reprocessing steps are now complete, congrats.

A.5 Intermediate Analysis

The intermediate analysis steps involve extracting radial profiles and spectra from the observations. These radial profiles form the basis for the final analysis steps of the next section. One script, `make_profile.pl`, extracts both a cumulative counts profile and a surface brightness profile. In the options section of the script you specify the size of the annular bins used to extract the profiles. For the cumulative counts profile I recommend 2 pixel width bins, and either 5 pixel or 10 pixel width bins for the surface brightness profiles. For the surface brightness profiles you also need to specify the energy range for the extraction. There are many other options for this script which are detailed in the program header.

```
[linux]% perl make_profile.pl reference.list
or
[linux]% perl make_multiprof.pl dub_reference.list
```

Depending on the number of counts in the observation, this step can take a few minutes or a few hours. The script also outputs plots of the two profiles which should be viewed to ensure everything ran correctly.

Now run the script `exp_corr.pl` which extracts a radial profile from the exposure map and will be used for exposure correcting radial profiles later on. As usual, set the options in the header, specifically the bin size of the profile to extract. The bin size needs to match that of the surface brightness profile just extracted. It is possible to extract multiple exposure profiles since the bin size is amended to the output file name. This step is fast, so extracting profile for bin sizes of 5, 10, or 20 pixels does not take long.

```
[linux]% perl exp_corr.pl reference.list
or
[linux]% perl multiexp_corr.pl dub_reference.list
```

With the cumulative profile, it is now possible to create annuli for the temperature profile. The script `make_annuli_reg.pro` is used to make the annuli. The cumulative profile is divided up into annular bins containing a minimum number of counts and then these bins are output as region files later used to extract spectra. The entries in the 'Mincts' column of the reference file are used to set the minimum number of counts. I typically run the script with all options set to "no" (meaning only mock regions are produced) and view the output plot to ensure the number and spacing of the bins is appropriate for the cluster in question. What is appropriate? Well, too many closely spaced annuli for a symmetric peaked cluster is redundant, and too few widely spaced annuli for a complex cluster is insuffcient, unless of course there are not enough counts to produce more bins. After ensuring the number of annuli produced is agreeable, run the script with the options set to "yes". **WARNING:** by default, the script deletes all annuli and associated spectral files. If you run this script after having extracted spectra, be sure to set `mkbackup` to "yes" AND provide the path to a valid, existing back-up directory, `bkdir`, this will save those existing spectra.

```
[linux]% idl
IDL> make_annuli_reg, 'reference.list'
or
IDL> make_multiannuli_reg, 'reference.list'
```

A whole ensemble of individual region files with the specified name will be output by this script. With these region files extracting spectra is straightforward, simply run the script `extract_spectra.pl`. This script has a number of important options which are detailed in the script header.

```
[linux]% perl extract_spectra.pl reference.list
```

If there have been no errors, then you should have radial profiles and spectra for each ObsID in the reference file, congratulations.

A.6 Final Analysis

The final steps in the analysis process are normalizing the background spectra for differences between the blank-sky background and observation background hard-particle count rates, extracting and fitting residual spectra for the local soft background, fitting the cluster spectra, and running the master IDL routine that produces entropy profiles. An explanation of why and how background adjustments are made is presented in Chapter 2.

A.6.1 Spectral Adjustments and Fitting

The hard-particle background is changing as a function of time. Thus, the strength of this background component for the epoch in which the blank-sky backgrounds were taken will be different from when the observations were taken. The first step in accounting for this difference involves running the script bgd_ratio.pl which will output the ratio of observation to blank-sky 9.5-12.0 keV count rates.

```
[linux]% perl bgd_ratio.pl reference.list
```

The script outputs a file containing these ratios. Keep this file someplace which is easily accessible as a later script will be querying this list to normalize the spectra.

To account for the spatially varying Galactic soft-component you must extract soft-residuals. Soft-residuals are the leftovers of subtracting a blank-sky spectrum from an observation spectrum both extracted from the same part of the sky and far from the cluster emission. The first step is to clean-up the off-axis observation chips of all point and diffuse sources. This step can be performed blind because if too many sources are removed it does not matter.

```
[linux]% perl addbg_rm_pt_src.pl reference.list
```

The soft-residual spectra are output from this script.

Prior to fitting any spectra all background spectra need to be normalized. This is done quickly by specifying the names of the spectra to be normalized in the script `adj_backscal.pl` and then running it.

```
[linux]% perl adj_backscal.pl reference.list
```

Normalization is applied by adjusting the header keyword `BACKSCAL` in the spectrum. The `BACKSCAL` keyword is related to the final background subtracted spectrum of an observation by

$$SPEC_{ctr} = \frac{SRC_{cts}}{SRC_{exp}} - \frac{BGD_{cts}}{BGD_{exp}} \cdot \frac{1}{BGD_{scal} \cdot SRC_{scal}} \tag{A.1}$$

where the abbreviations 'SRC' $\rightarrow$ source, 'BGD' $\rightarrow$ background, 'ctr' $\rightarrow$ count rate, 'cts' $\rightarrow$ counts, 'exp' $\rightarrow$ exposure time, and 'scal' $\rightarrow$ `BACKSCAL`. The `BACKSCAL` keyword is defined as the detector area over which the spectrum was extracted, divided by the total detector area. Adjustment of the blank-sky background `BACKSCAL` value follows directly from the above equation by multiplying the existing value of `BACKSCAL` by a correction factor, η, which is related to the ratio of the count rate in the 9.5-12.0 keV range of the observation to the blank-sky background by

$$\eta = (\frac{OBS_{ctr}}{BGD_{ctr}})^{-1}. \tag{A.2}$$

Each background spectrum is copied into a new file before this correction is applied so that reversal at a later date is possible.

Now that the spectra are all adjusted, the fitting can begin. There are a large number of options in spectral fitting and these are detailed in the individual script's header. In addition, intepreting the results of the fitting requires more discussion than is useful here. The order in which fitting is done is important since the master spectral fitting routines need output from the fitting of the soft-residuals.

```
[linux]% perl fit_sofex.pl reference.list <spectral model>

[linux]% perl fit_projected.pl reference.list <spectral model>

or

[linux]% perl fit_simulta.pl dub_reference.list <spectral model>
```

The output of these scripts are data tables with the spectral fits for each annulus associated with each ObsID. With radial profiles in-hand and spectral analysis complete, it is now possible to calculate many more physical properties of a cluster.

A.6.2 GENERATING ENTROPY PROFILES

So here it is, the end of a long journey. Your CIAO-Fu is good, congratulations. The master program which performs the deprojection, derives electron gas density, pressure, entropy, mass (not to be trusted), and cooling time is `kfitter.pro`. This program has a handler program `run_kfit.pro` which makes batch analysis simpler. These programs have their own `README` files which have not been duplicated here. After running `kfitter.pro` you will have a suite of data tables and plots for each cluster which are publication ready. If desired, I have a whole suite of IDL programs to offer which perform additional analysis, output many more plots, and handle odds-n-ends type tasks like making web pages.

APPENDIX B:
CO-AUTHORED PUBLICATIONS

Listed below are references to publications for which I have contributed work which is not included in this dissertation.

Donahue et al. (2006): The X-ray analysis, entropy profiles, and literature comparison for the nine clusters discussed in this paper were completed by me.

Donahue et al. (2007): I provided some of the analysis for the *Chandra* X-ray data discussed in the paper.

Sharpee et al. (2007): I analyzed the double echelle spectrograph data taken with the MIKE instrument on the Magellan Telescope. The observations were of IC 2501, IC 4191, and NGC 2440.

Voit et al. (2008): The X-ray results presented in this paper were taken from dissertation.